AD A

COUPLED SIMULATION OF VEHICLE DYNAMICS AND TANK SLOSH
Phase 1 Report
Testing And Validation Of Tank Slosh Analysis

INTERIM REPORT
TFLRF NO. 364

Prepared by

Glenn R. Wendel
Steven T. Green
Russell C. Burkey

Prepared for

U. S. ARMY TACOM
Attn: AMSTA-DSA-FP-PW
Warren, Michigan 48397-5000

Under Contract to

U. S. ARMY TACOM
Attn: AMSTA TR-D/210
Warren, Michigan 48397-5000

TACOM Contract No. DAAE07-99-C-L053 (Work Directive 14)

SwRI Project No. 03.03227.14

Approved for public release; distribution unlimited

September 2002

AD A

COUPLED SIMULATION OF VEHICLE DYNAMICS AND TANK SLOSH
Phase 1 Report
Testing And Validation Of Tank Slosh Analysis

INTERIM REPORT
TFLRF NO. 364

Prepared by

Glenn R. Wendel
Steven T. Green
Russell C. Burkey

Prepared for

U. S. ARMY TACOM
Attn: AMSTA-DSA-FP-PW
Warren, Michigan 48397-5000

Under Contract to

U. S. ARMY TACOM
Attn: AMSTA TR-D/210
Warren, Michigan 48397-5000

TACOM Contract No. DAAE07-99-C-L053 (Work Directive 14)

SwRI Project No. 03.03227.14

Approved for public release; distribution unlimited

September 2002

Approved:

Gary L. Stecklein, Director
Vehicle Systems Research Department

This report must be reproduced in full, unless SwRI approves a summary or abridgement.

REPORT DOCUMENTATION PAGE

Form Approved
OMB No. 0704-0188

Public reporting burden for this collection of information is estimated to average 1 hour per response, including the time for reviewing instructions, searching existing data sources, gathering and maintaining the data needed, and completing and reviewing this collection of information. Send comments regarding this burden estimate or any other aspect of this collection of information, including suggestions for reducing this burden to Department of Defense, Washington Headquarters Services, Directorate for Information Operations and Reports (0704-0188), 1215 Jefferson Davis Highway, Suite 1204, Arlington, VA 22202-4302. Respondents should be aware that notwithstanding any other provision of law, no person shall be subject to any penalty for failing to comply with a collection of information if it does not display a currently valid OMB control number. **PLEASE DO NOT RETURN YOUR FORM TO THE ABOVE ADDRESS.**

1. REPORT DATE *(DD-MM-YYYY)*
September 30, 2002

2. REPORT TYPE
Interim Report

3. DATES COVERED *(From - To)*
February 2002 – July 2002

4. TITLE AND SUBTITLE
Coupled Simulation of Vehicle Dynamics and Tank Slosh
Phase I: Testing and Validation of Tank Slosh Analysis

5a. CONTRACT NUMBER
DAAE-07-99-C-L053

5b. GRANT NUMBER

5c. PROGRAM ELEMENT NUMBER

6. AUTHOR(S)
Glenn Wendel, Steve Green and Russell Burkey

5d. PROJECT NUMBER
03-03227.14

5e. TASK NUMBER

5f. WORK UNIT NUMBER
14

7. PERFORMING ORGANIZATION NAME(S) AND ADDRESS(ES)
Southwest Research Institute™
P.O. Drawer 28510
San Antonio, Texas 78228-0510

8. PERFORMING ORGANIZATION REPORT NUMBER
IR 364

9. SPONSORING / MONITORING AGENCY NAME(S) AND ADDRESS(ES)
U. S. Army TACOM
AMSTA TR-D/210
6501 E. 11 Mile Road
Warren, MI 48397-5000

U. S. Army TACOM
AMSTA DSA-FP/FW
6501 E. 11 Mile Road
Warren, MI 48397-5000

10. SPONSOR/MONITOR'S ACRONYM(S)
TARDEC, TACOM

11. SPONSOR/MONITOR'S REPORT NUMBER(S)

12. DISTRIBUTION / AVAILABILITY STATEMENT
A: Approved for Public Release; Distribution Unlimited

13. SUPPLEMENTARY NOTES

14. ABSTRACT

Computer simulation of vehicle dynamics has become a valuable tool in the design of vehicles. They are, however, unable to accurately simulate the complex dynamics of fluid "sloshing" in a tank on the vehicle. Computational Fluid Dynamics (CFD) analysis software is available that can predict fluid slosh, however, the use of this software in accurately predicting fluid slosh for a military vehicle application has not been demonstrated.

This is the first phase of a multiphase program to develop and demonstrate the use of CFD analysis, coupled with vehicle dynamics analysis, to more accurately predict the dynamics of a fluid transport system. The objective of this phase is to validate the CFD analysis in predicting slosh dynamics on a tank subjected to motions of a vehicle encountering typical maneuvers. To accomplish this, a one-quarter-scale model of a TULD tank was constructed, as well as a test fixture to simulate a five-ton FMTV truck. The reaction forces and the fluid motions of the CFD analysis and the laboratory test were compared for six simulated vehicle maneuvers including lane changes and bumps.

The CFD analysis was conducted with the commercially available software package, FLOW-3D®. The net fluid force and moment predictions were added to the force and moment predictions of a rigid body dynamic analysis of the empty tank alone to compare to the corresponding measured values for the test tank.

Overall, the results show that CFD can successfully be applied to the study of fluid motions and the fluid-structure interactions in truck-mounted water transport tanks. There is good correlation between the predicted and measured roll moment. Given the rapid turnaround time for the CFD simulations presented here, the outlook is encouraging for coupling a vehicle rigid body dynamics analysis to a fluid dynamics analysis for a high fidelity simulation of the complete vehicle response to maneuvers. It is recommended that the next phase be conducted, which is to couple the CFD analysis software with the vehicle dynamics software.

15. SUBJECT TERMS
Computational Fluid Dynamics (CFD) Tank Slosh Vehicle Dynamics Fluid Transport

16. SECURITY CLASSIFICATION OF:			17. LIMITATION OF ABSTRACT	18. NUMBER OF PAGES	19a. NAME OF RESPONSIBLE PERSON
					Luis Villahermosa
a. REPORT	b. ABSTRACT	c. THIS PAGE		57	19b. TELEPHONE NUMBER *(incl area code)* 586-574-4207

Standard Form 298 (Rev. 8-98)
Prescribed by ANSI Std. Z39.18

EXECUTIVE SUMMARY

Computer simulation of vehicle dynamics has become a valuable tool in the design of vehicles. They are, however, unable to accurately simulate the complex dynamics of fluid "sloshing" in a tank on the vehicle. Computational Fluid Dynamics (CFD) analysis software is available that can predict fluid slosh, however, the use of this software in accurately predicting fluid slosh for a military vehicle application has not been demonstrated.

This is the first phase of a multiphase program to develop and demonstrate the use of CFD analysis, coupled with vehicle dynamics analysis, to more accurately predict the dynamics of a fluid transport system. The objective of this phase is to validate the CFD analysis in predicting slosh dynamics on a tank subjected to motions of a vehicle encountering typical maneuvers. To accomplish this, a one-quarter-scale model of a tank was constructed, as well as a test fixture, to dynamically test the tank under simulated maneuvers. A TULD tank was simulated half full of water mounted on a five ton FMTV truck at a scale factor of 1/4.4. The reaction forces and the fluid motions of the CFD analysis and the laboratory test were compared for the following simulated vehicle maneuvers:

- AVTP Lane Change at 20 mph
- AVTP Lane Change at 40 mph
- 9" Half-Round Symmetric Bump at 10 mph
- 12" Half-Round Symmetric Bump at 5 mph
- 9" Trapezoidal Asymmetric Bump at 15 mph
- 12" Trapezoidal Asymmetric Bump at 10 mph

The CFD analysis was conducted with the commercially available software package, FLOW-3D®. The net fluid force and moment predictions were added to the force and moment predictions of a rigid body dynamic analysis of the empty tank alone to compare to the corresponding measured values for the test tank.

In this effort, the parameter of primary importance is considered to be the moment about the vehicle roll axis. From that standpoint, there is good correlation between the predicted and measured roll moment. The main features of the tank and liquid dynamic behavior are closely predicted, but the predicted peak roll moment deviates from the measured value, depending on the harshness of the maneuver. There is corresponding good agreement between the recorded fluid motion and the animation of the CFD predictions for the fluid configuration during the maneuvers.

Overall, the results presented here show that CFD can successfully be applied to the study of fluid motions and the fluid-structure interactions in truck-mounted water transport tanks. In some cases, the fluid sloshing effects are significant. As has been demonstrated in some accidents, the vehicle dynamics and fluid dynamics can be strongly coupled. Given the rapid turnaround time for the CFD simulations presented here, the outlook is encouraging for coupling a vehicle rigid body dynamics analysis to a fluid dynamics analysis for a high fidelity simulation of the complete vehicle response to maneuvers.

As an example of the correlation of the CFD-predicted results to the test results, the following plot shows the roll moment for each case that the tank with fluid imparts on the vehicle as it negotiates an AVTP Lane Change at 40 mph. These results show that the comparison is very good, particularly at the start of the event and that the roll moments are significant.

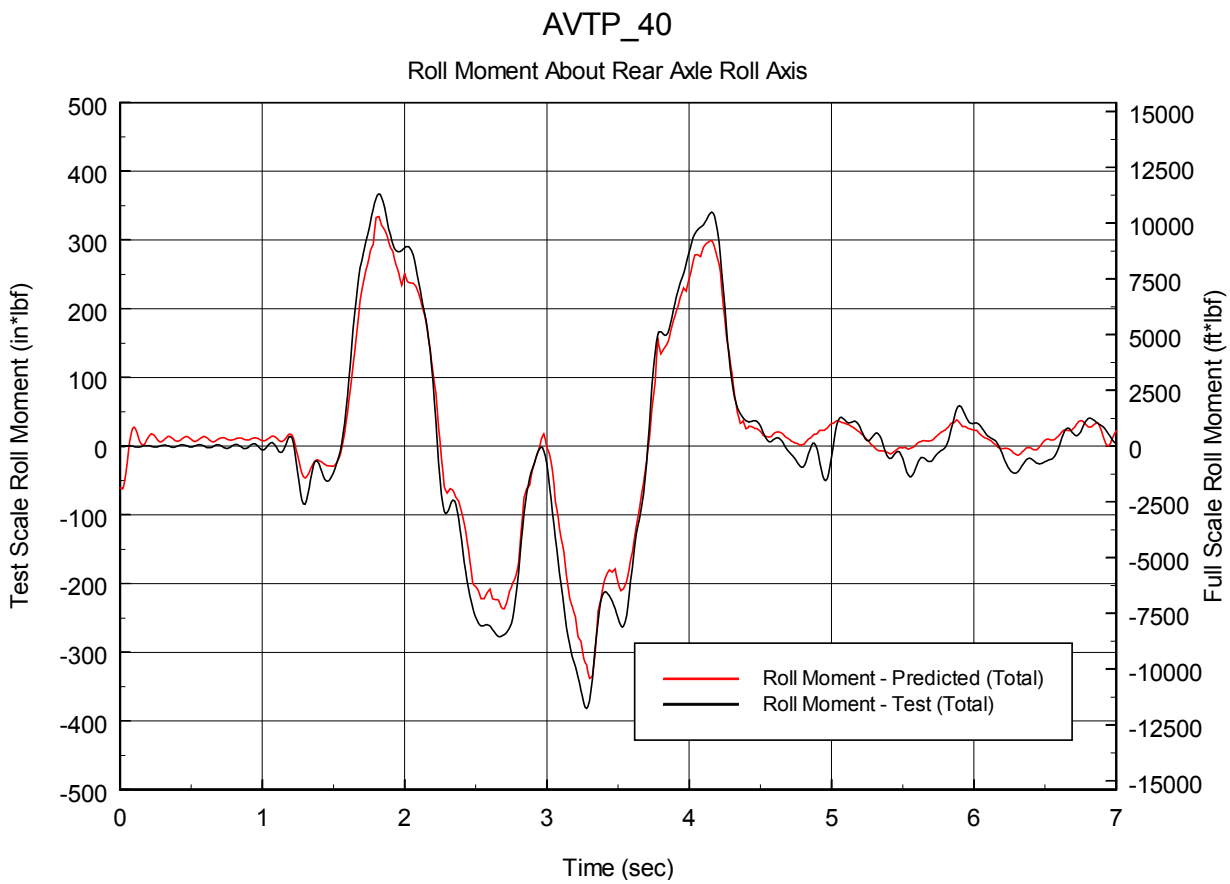

Rear Axle Roll Moment, 40-mph Lane Change.

The results of this study clearly demonstrate that the effect of fluid slosh is significant, which will have a significant affect on vehicle dynamics. It is recommended that we proceed to the next phase, which is to couple the CFD analysis software with the vehicle dynamics software. The computational time required to perform the CFD analysis was relatively short, which should have only a small increase on the overall computational time of a coupled simulation. There is also a recommendation to further improve the correlation of the CFD analysis to the test data by increasing the fidelity of the model.

TABLE OF CONTENTS

Section **Page**

EXECUTIVE SUMMARY ..... **I**

LIST OF ILLUSTRATIONS ..... **IV**

1. INTRODUCTION **1-1**

2. TEST PROGRAM **2-1**

2.1 TEST SCALE 2-1
2.2 TEST RIG 2-2
2.3 MOTION SIMULATION 2-5
2.3.1 Sensor Calibration 2-5
2.4 UNCERTAINTY ESTIMATE 2-7
2.5 TEST MEASUREMENTS 2-8

3. SLOSH LOAD PREDICTIONS AND DATA ANALYSIS **3-1**

3.1 CFD MODEL SETUP 3-1
3.1.1 Computational Mesh 3-1
3.1.2 Fluid Properties 3-2
3.1.3 Motion Description 3-2
3.1.4 Grid Independence Assessment 3-3
3.2 DATA ANALYSIS 3-3
3.2.1 Measured and Predicted Loads 3-3
3.2.2 Roll Moment Comparison 3-3
3.2.3 Fluid Motion Comparisons 3-8

4. CONCLUSIONS AND RECOMMENDATIONS **4-1**

5. REFERENCES **5-1**

APPENDIX A: ROLL APPROXIMATION FOR LANE CHANGE MANEUVERS **A-1**

APPENDIX B: UNCERTAINTY ANALYSIS **B-1**

APPENDIX C: MEASURED AND PREDICTED TANK LOADS **C-1**

LIST OF ILLUSTRATIONS

Figure **Page**

Figure 2.1. Test Setup 2-3

Figure 2.2. Test Setup Drawing 2-4

Figure 3.1. Computational Mesh Definition 3-2

Figure 3.2. Rear Axle Roll Moment, 20-mph Lane Change 3-4

Figure 3.3. Rear Axle Roll Moment, 40-mph Lane Change 3-5

Figure 3.4. Rear Axle Roll Moment, 9” Trapezoidal Bump at 15 mph 3-5

Figure 3.5. Rear Axle Roll Moment, 12” Trapezoidal Bump at 10 mph 3-6

Figure 3.6. Rear Axle Roll Moment, 9” Half Round Bump at 10 mph 3-7

Figure 3.7. Rear Axle Roll Moment, 12” Half Round Bump at 5 mph 3-7

Figure 3.8. Fluid Configuration for 20-mph Lane Change 3-9

Figure 3.9. Fluid Configuration for 12” Trapezoidal Bump at 10 mph 3-10

Figure A.1. Lane Change Roll Profile Development (view from rear of vehicle) A-1

Figure A.2. 20-mph Lane Change (AVTP_20) Lateral (x-direction) Force Comparison A-2

Figure A.3. 40-mph Lane Change (AVTP_40) Lateral (x-direction) Force Comparison A-3

1. INTRODUCTION

Fluid transport systems have an inherent concern with dynamic stability since the fluid motion, or "sloshing", introduces an additional large mass degree of freedom to the vehicle system. Vehicle motions induced by the terrain and/or by the operator (steering, braking, and accelerating) cause the fluid in a transport tank, supported by the vehicle, to move relative to the tank, causing reaction loads on the tank and the vehicle that are much different than static loads. If the tank and the vehicle system are not properly designed, the dynamic phasing of these loads can result in vehicle rollover or a loss of control. There are a wide range of conditions that need to be considered as possible unstable conditions including various terrain, maneuvers, and fluid fill level. Instability is a concern for tanks mounted directly on a vehicle, as well as for tanks mounted on trailers and pulled by a vehicle.

The potential instability of a vehicle either carrying a tank or towing a trailer with a tank is a significant safety concern, particularly when handling flammable fluids. Fluid spills can also be an environmental hazard.

Current vehicle dynamics modeling software, such as the LMS DADS software, is capable of providing good predictions of dynamic performance of typical vehicles, however, they do not include an accurate method of representing the dynamics of a fluid in a tank.

Traditional methods of representing fluid slosh dynamics are to use a "pendulum" model in which the mass of the fluid is represented mathematically as a concentrated mass swinging from a pendulum with a certain length that will represent the fluid's natural frequency. The pendulum model is incorporated into a vehicle dynamics model to produce a coupled simulation. The drawback of a pendulum model is that it is only good for linear fluid motion, or when the fluid surface remains flat. When waves develop, when the fluid rolls over, or when there is a separation of fluid, the pendulum model is not accurate. It is also very difficult to use the pendulum model to simulate a tank with baffles.

With the current advancements in fluid dynamic modeling software, more commonly referred to as "Computational Fluid Dynamics" (CFD) analysis tools, it is possible to accurately represent the dynamic motions of free surface fluids, or sloshing, including waves and fluid separation. This type of analysis is generally referred to as a "volume of fluid" analysis, in which there is a finite fluid volume that is accounted for as it is exposed to motions from a container of a larger volume.

The motions of the vehicle affect the motion of the fluid in the tank; and, consequently, the motion of the fluid in the tank imparts loads on the body of the vehicle that affects its motion. These are "coupled" dynamic motions and they need to be modeled as a coupled system. There is no practical means of modeling them separately. The ideal modeling tool would be one that couples a vehicle dynamics model with a CFD analysis of the fluid. Since there is no known modeling tool commercially available that can perform this type of analysis, the ultimate goal of this overall program is to develop the means for performing this type of analysis using commercially available software and providing the appropriate links to the two software packages. The first step in this process is the purpose of this project (Phase 1) - to validate the accuracy of the CFD analysis method for modeling fluid slosh. The results of Phase 1 are summarized in this report.

The validation was accomplished by simulating the fluid motions in a tank on a vehicle using the FLOW-3D® CFD analysis software and comparing the resulting fluid forces to the measured forces of a laboratory test. The validation tests were performed on 1/4.4-scale test setup that replicated the motions of an FMTV truck with a 600-gallon tank mounted on its bed running through several maneuvers at two different speeds. The motions were defined by DADS simulations of the vehicle performing these maneuvers.

Following this validation step, the next step (Phase 2) is to couple the two analysis packages, the DADS vehicle dynamics software, and the CFD analysis software, so that they will perform their respective analyses in parallel, feeding each other the required force and displacement information. The resulting coupled simulation will most accurately predict actual vehicle dynamics of a tank-type vehicle and its sloshing fluid. Phase 3 is planned to be the validation of a full-scale model of the tank on an actual vehicle in a field test or on a dynamic simulator. Phase 4 will include the application of the coupled simulation system to optimizing the design of a vehicle and tank.

The coupled simulation system of vehicle dynamics and tank slosh developed in this program will have significant impact on the development of fluid transport systems for both military applications as well as commercial applications.

2. TEST PROGRAM

The approach to conducting a laboratory test for the purpose of validating the CFD analysis was to select a vehicle and a tank to be simulated, and build a scale model of this tank and a simple actuation system to impart motions on the tank that are typical of actual vehicle maneuvers. The objective was to impose motions on the tank that were representative of the primary motions for the various maneuvers as a baseline for validating the results of the CFD analysis for the exact same motions.

The test setup was simplified in design and only included two actuators attached to a subframe to provide the primary motions to the tank. These two actuators were located at the two rear spring locations of the vehicle and a pivot point was located at the front axle roll center.

It was decided between TACOM and Southwest Research Institute that the test setup should simulate a 5-ton FMTV truck and that it would have a 600-gallon TULD tank mounted on it. A scale model of a TULD tank was fabricated and subjected to motion profiles that approximate the following full-scale maneuvers (the test code numbers are given in parentheses):

- AVTP Lane Change at 20 mph (AVTP_20)
- AVTP Lane Change at 40 mph (AVTP_40)
- 9" Half-Round Symmetric Bump at 10 mph (HR_9_10)
- 12" Half-Round Symmetric Bump at 5 mph (HR_12_5)
- 9" Trapezoidal Asymmetric Bump at 15 mph (T_9_15)
- 12" Trapezoidal Asymmetric Bump at 10 mph (T_12_10)

This section describes the laboratory tests of the scaled tank and the procedures used to compute the combined dynamic loads applied to the tank and the fluid.

2.1 TEST SCALE

A scaling analysis was performed to provide a basis for applying the simulated full-scale FMTV motions to a laboratory-scale test article. While there are many approaches to a scaling analysis of the tank motions, the Buckingham Pi theorem, as described by Baker et al. [1991], is used here.

The fluid-related force resulting from a response to a specified motion is assumed to be of the form

$$F = f\left[L_{tank}, \rho, g, L_{bump}, V_{vehicle}, \omega_{fluid}\right] \tag{2.1}$$

where F = force response to tank motion
L_{tank} = characteristic tank dimension for dominant fluid motion
ρ = fluid density
g = acceleration due to gravity
L_{bump} = characteristic bump or maneuver dimension
$V_{vehicle}$ = vehicle velocity
ω_{fluid} = fluid motion natural frequency

Applying the Buckingham Pi methods results in the following transformation of Eq. 2.1 into a dimensionless expression

$$\frac{F}{L_{tank}\rho V_{vehicle}^2} = f\left[\frac{L_{tank}g}{V_{vehicle}^2}, \frac{L_{tank}}{L_{bump}}, \frac{L_{tank}\omega_{fluid}}{V_{vehicle}}\right] \tag{2.2}$$

This relationship states that as long as the values of the dimensionless parameters on the right side of Eq. 2.2 are the same for the model and the full-scale tank, the model response force can be scaled to the full-scale tank according to the left side of Eq. 2.2.

The geometric scale factor for the test article is defined as λ; that is, $(L_{tank})_{model} = \lambda(L_{tank})_{actual}$. The geometric scale factor used in the current test program is λ=1/4.4. The test fluid, water, is the same as that in the full-scale tank, and the acceleration due to gravity is the same for both the model and the full-scale tank. So, from Eq. 2.2, it can be seen that the scale factors for the kinematic and dynamic parameters of interest are as follows:

$\lambda_{velocity}$ = $\lambda^{1/2}$ (from the term, $L_{tank}g/V^2_{vehicle}$)
λ_{force} = λ^3 (from the term, $F/L_{tank}\rho V^2_{vehicle}$)
λ_{time} = $\lambda^{1/2}$ (from the term, $L_{tank}\omega_{fluid}/V_{vehicle}$)
λ_{mass} = λ^3 (from the fact that mass is proportional to L^3_{tank})
$\lambda_{acceleration}$ = 1 (from $\lambda_{acceleration} = \lambda_{force}/\lambda_{mass}$)
λ_{moment} = λ^4 (from $\lambda_{moment} = \lambda_{force}\cdot\lambda$)

In summary, the model tank displacements are scaled in accordance with the model geometric scale factor. The time over which the motion occurs should be multiplied by the square root of the geometric scale factor. The resulting velocity scale of the model motion is automatically satisfied and the accelerations experienced by the model are identical to those in the full-scale tank. Finally, the full-scale force is obtained by multiplying the model force by the cube of the geometric scale factor.

2.2 TEST RIG

A picture of the test setup is given in Figure 2.1. The test setup consists of a clear plastic scale model tank attached to a rigid aluminum frame by three multi-axis load cells. Each multi-axis load cell simultaneously measures forces in three directions. As explained in detail in the calibration discussion, these nine forces can be combined to give total forces and moments about the center of the tank.

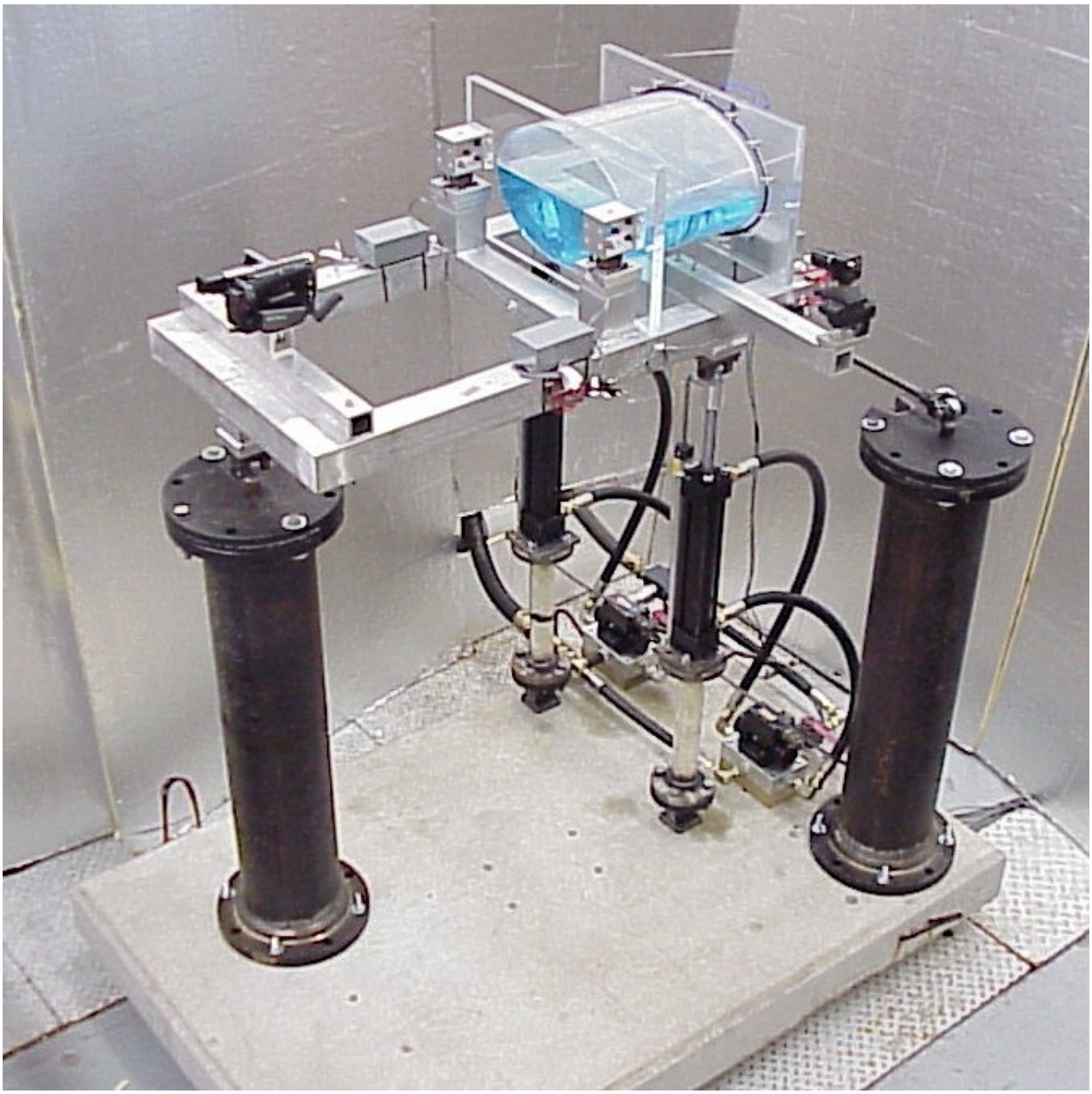

Figure 2.1. Test Setup.
The test setup consists of a clear plastic scale model tank attached to a rigid aluminum frame by three multi-axis load cells driven by a position-controlled servo hydraulic system. (Data acquisition cabling removed for clarity).

Figure 2.2 shows a drawing of the test setup in which the load cell locations and the coordinate systems used in the testing and analysis are defined. The inertial coordinate system (XYZ) is centered at the fixed point of rotation, which coincides with the location of the front axle roll center in the scaled test setup. The body-fixed coordinate system, about which forces and moments are summed, is located at the geometric center of the test tank.

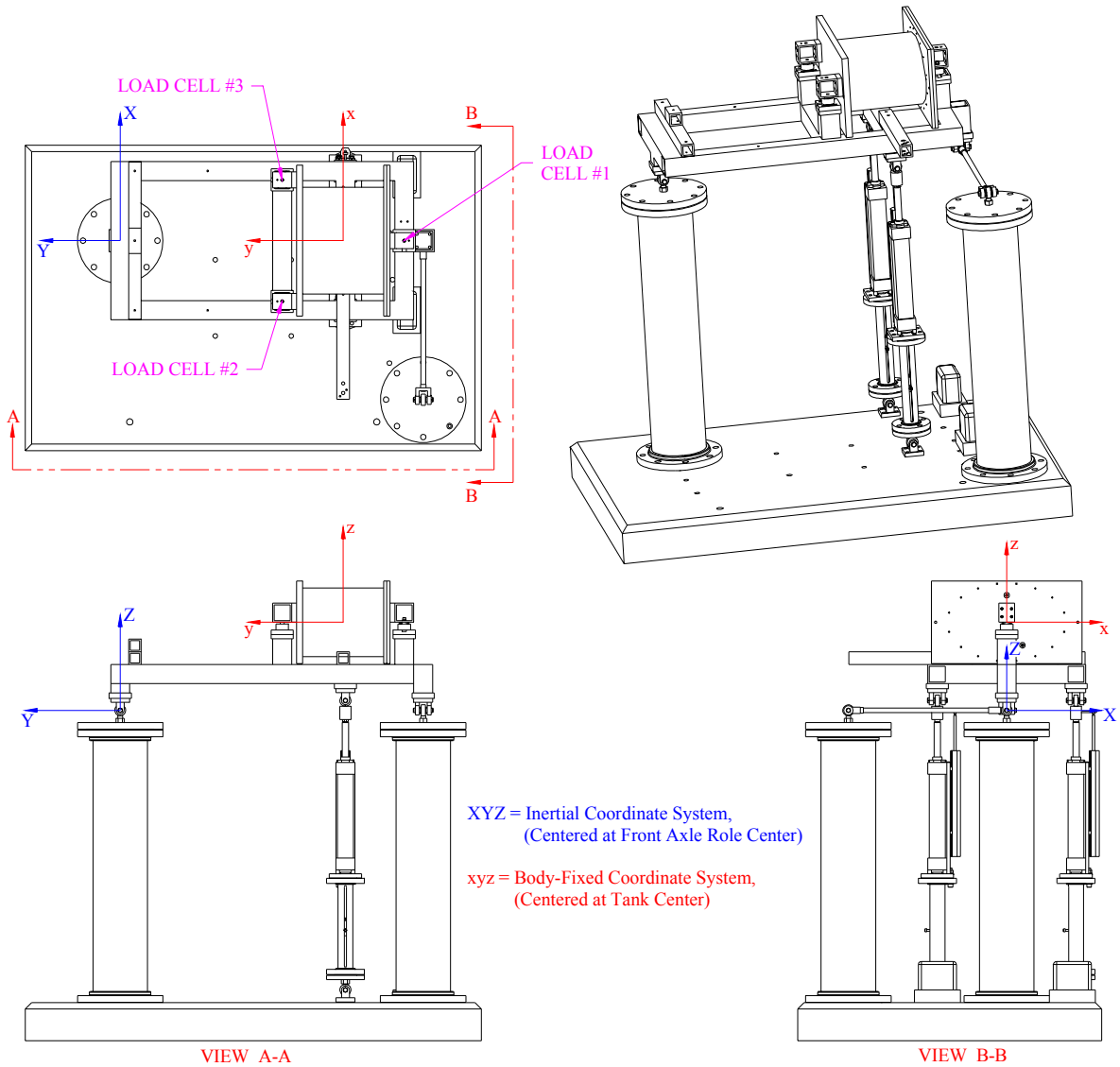

Figure 2.2. Test Setup Drawing.
The load cell locations and the coordinate systems used in the testing and analysis are defined as shown.

The rigid frame is supported by two hydraulic cylinders and two fixed stands. The hydraulic cylinders are each part of an independent, position-controlled servo loop. The control software, written in LabVIEW, sends displacement profile commands to two servo amplifiers that send the appropriate signal to two servo valves in order to control the positions of the hydraulic cylinders. Displacement transducers mounted to the hydraulic cylinders provide the feedback required to obtain closed-loop servo control.

One fixed stand allows the frame to rotate about a ball joint located at the front, center point of interest. A tie rod connects the frame at the vehicle rear axle roll center to the second fixed stand in order to provide lateral support to the test setup. (The two hydraulic cylinders are mounted using spherical rod ends at the top and bottom. Therefore, the test setup would be unstable in the lateral direction without the tie rod).

A scale model tank assembly was constructed out of clear acrylic plastic. Its axial cross-section was of an elliptical shape to closely replicate the TULD tank shape. The ends of the tank were flat, whereas the TULD tank ends are slightly rounded.

Three uniaxial DC accelerometers are mounted to the tank assembly in order to measure acceleration in the x, y, and z directions. The load cell, accelerometer, and displacement transducer data is recorded using a simple LabVIEW data acquisition program and A/D board installed in the data acquisition computer. Two cameras mounted to the frame record the fluid motion during testing. A video mixer allows the video signals to be recorded simultaneously on one VCR tape.

2.3 MOTION SIMULATION

TACOM provided Southwest Research Institute™ with displacement, velocity, and acceleration time histories at three points of interest on the FMTV truck based on a dynamic simulation of the FMTV truck completing each of the maneuvers to be studied. These three points of interest included:

1. center, front point of interest – front axle roll axis, vehicle center

   (vehicle coordinate: x=0”, y=0”, z=29.43”)
2. right, rear point of interest – rear axle roll axis, vehicle right side,

   (vehicle coordinate: x=+48”, y=-161.4”, z=36.14”)
3. left, rear point of interest – rear axle roll axis, vehicle left side,

   (vehicle coordinate: x=-48”, y=-161.4”, z=36.14”)

The time history data was used to develop cylinder displacement command profiles. For each bump maneuver, the relative vertical (z-direction) displacements of the right-rear and left-rear points of interest with respect to the front, center point of interest were scaled ($1/\lambda$) to create the desired displacement command profile. For each lane change maneuver, the dominant acceleration - lateral (x-direction) acceleration - was simulated with a pure rolling motion. The roll angle profile was developed such that the sum of the body force acceleration due to tilting the tank in the gravity field and the tangential acceleration due to the rolling motion would match average lateral acceleration from the FMTV truck simulation. A complete derivation of the lane change command profile is given in Appendix A. For all maneuvers, time was scaled ($1/\lambda^{0.5}$), as required.

2.3.1 Sensor Calibration

The load cell assembly was calibrated statically with the tank assembly installed on the frame. The sensitivity of the pertinent force sensors to the three force components (Fx, Fy, Fz) and three moment components (Mx, My, Mz) was measured by applying forces and moments via calibrated force instrumentation. The static calibration was used to set the nominal gain of the force sensor amplifiers to maintain the amplifier output voltage within the maximum allowable range of 0 to 5 volts.

The calibration data were used to develop the transfer function between the nine force sensor measurements and the desired forces and moments. This transfer function included the

effects of crosstalk between applied loads and the unintended off-axis sensor outputs. This transfer function was developed as follows.

First, the output from each of the nine force sensor measurements is assumed to be the sum of the effects from all six of the possible applied loads,

$$V_{x1} = K_{x1.Fx}F_x + K_{x1.Fy}F_y + K_{x1.Fz}F_z + K_{x1.Mx}M_x + K_{x1.My}M_y + K_{x1.Mz}M_z \tag{2.2a}$$

$$V_{x2} = K_{x2.Fx}F_x + K_{x2.Fy}F_y + K_{x2.Fz}F_z + K_{x2.Mx}M_x + K_{x2.My}M_y + K_{x2.Mz}M_z \tag{2.2b}$$

$$V_{x3} = K_{x3.Fx}F_x + K_{x3.Fy}F_y + K_{x3.Fz}F_z + K_{x3.Mx}M_x + K_{x3.My}M_y + K_{x3.Mz}M_z \tag{2.2c}$$

$$V_{y1} = K_{y1.Fx}F_x + K_{y1.Fy}F_y + K_{y1.Fz}F_z + K_{y1.Mx}M_x + K_{y1.My}M_y + K_{y1.Mz}M_z \tag{2.2d}$$

$$V_{y2} = K_{y2.Fx}F_x + K_{y2.Fy}F_y + K_{y2.Fz}F_z + K_{y2.Mx}M_x + K_{y2.My}M_y + K_{y2.Mz}M_z \tag{2.2e}$$

$$V_{y3} = K_{y3.Fx}F_x + K_{y3.Fy}F_y + K_{y3.Fz}F_z + K_{y3.Mx}M_x + K_{y3.My}M_y + K_{y3.Mz}M_z \tag{2.2f}$$

$$V_{z1} = K_{z1.Fx}F_x + K_{z1.Fy}F_y + K_{z1.Fz}F_z + K_{z1.Mx}M_x + K_{z1.My}M_y + K_{z1.Mz}M_z \tag{2.2g}$$

$$V_{z2} = K_{z2.Fx}F_x + K_{z2.Fy}F_y + K_{z2.Fz}F_z + K_{z2.Mx}M_x + K_{z2.My}M_y + K_{z2.Mz}M_z \tag{2.2h}$$

$$V_{z3} = K_{z3.Fx}F_x + K_{z3.Fy}F_y + K_{z3.Fz}F_z + K_{z3.Mx}M_x + K_{z3.My}M_y + K_{z3.Mz}M_z \tag{2.2i}$$

where V_{x1} is the output from the x-component of the force sensor in position 1, F_x is the applied x-direction force, and $K_{x1.Fx}$ is the calibration factor for this particular sensor output for the applied load, F_x. The other terms are defined similarly.

The individual *K*-terms are computed by applying a single isolated force or moment along each of the load cell assembly axes. The *K*-terms are the slope of each sensor's output with respect to the applied force or moment.

These equations represent nine coupled equations in six unknowns. Considering the sensor layout and a static load balance for the load cell assembly, the following six equations can be obtained by judiciously combining particular equations from this set.

$$V_{fx} = V_{x1} + V_{x2} + V_{x3} \tag{2.3a}$$

$$V_{fy} = V_{y1} + V_{y2} + V_{y3} \tag{2.3b}$$

$$V_{fz} = V_{z1} + V_{z2} + V_{z3} \tag{2.3c}$$

$$V_{mx} = -V_{z1} + V_{z2} + V_{z3} \tag{2.3d}$$

$$V_{my} = V_{z2} - V_{z3} \tag{2.3e}$$

$$V_{mz} = \left(-V_{y2} + V_{y3}\right)\frac{\Delta x_3}{\Delta y_1} + V_{x1} - V_{x2} - V_{x3} \tag{2.3f}$$

In these equations, V_{fx} represents the sum of the individual x-direction force sensor voltages and can be shown to be strongly related to the applied x-direction force. The other combination terms, V_{fy}, V_{fz}, V_{mx}, V_{my}, and V_{mz} are similarly defined. The lower case '*f*' and '*m*' are used here to distinguish these terms as voltages related to force and moment from the actual applied force and moment. The distance, Δx_3, is the absolute value of the x-direction coordinate for the sensor

in position 3 with respect to the center of the assembly ($\Delta x_1 = 0$; $\Delta x_2 = \Delta x_3$). Likewise, Δy_3, is the absolute value of the y-direction coordinate of the force sensor in position 1 with respect to the center of the assembly ($\Delta y_1 = \Delta y_2 = \Delta y_3$).

The right sides of Eq. (2.2) are combined in accordance with Eq. (2.3). With terms collected, the resulting equation set is cast in matrix form,

$$\begin{bmatrix} V_{fx} \\ V_{fy} \\ V_{fz} \\ V_{mx} \\ V_{my} \\ V_{mz} \end{bmatrix} = \mathbf{K} \begin{bmatrix} F_x \\ F_y \\ F_z \\ M_x \\ M_y \\ M_z \end{bmatrix} \tag{2.4}$$

The matrix, **K**, is a 6x6 matrix in which the terms are composed of the combinations of the *K*-terms in Eq. (2.2), in accordance with the algebra indicated in Eq. (2.3).

Finally, the applied forces and moments are computed from the measured voltages by inverting the matrix **K** and premultiplying the measured combination voltage terms (*i.e.*, measured voltage combinations). This methodology is applied to all the measured data from the tests to compute the applied forces and moments from the measurements acquired from the nine force sensor outputs.

2.4 UNCERTAINTY ESTIMATE

There are many sources of error, or uncertainty, in the measurement and processing of the force sensor voltage signals in order to arrive at the three net force and moment components described in this report. Among the sources of error are hysteresis and stability of the sensor elements, random errors in the electrical and digital instrumentation, linearity in converting the voltage signals to engineering units, and crosstalk between the sensor components. During the sensor calibration procedures, it was discovered that curve fit errors (i.e., engineering unit conversion linearity) and crosstalk were, by far, the dominant sources of uncertainty in the measurement of the loads on the sensor assembly. The results of the uncertainty analysis are listed below, and a complete discussion of the uncertainty analysis can be found in Appendix B.

The curve fit uncertainty ($U_{cf,Fx}$, $U_{cf,Fy}$, . . .) arises because the response of each of the nine sensors was not precisely linear with respect to the applied force and moment components. These uncertainty values are expressed as magnitudes of force and moment, since they are constant over the entire load range.

$U_{cf,Fx}$=2.3 lbf	$U_{cf,Mx}$=6.1 in*lbf
$U_{cf,Fy}$=4.5 lbf	$U_{cf,My}$=2.0 in*lbf
$U_{cf,Fz}$=0.3 lbf	$U_{cf,Mz}$=34 in*lbf

The crosstalk uncertainty ($U_{ct,Fx}$, $U_{ct,Fy}$, . . .) arises because the crosstalk elimination process (Section 2.3.1) is based on the nominal values of the sensor sensitivities and does not eliminate all of the crosstalk for all load levels and load combinations. The crosstalk uncertainty is an expression of the residual crosstalk that remains when the crosstalk elimination process is

performed. The analysis shows that there is no fixed value for the relative crosstalk uncertainty. The following maximum values from an example case (9" trapezoidal asymmetric bump [T_9_15]), however, are obtained.

$U_{ct,Fx}$=0.48 lbf	$U_{ct,Mx}$=1.4 in*lbf
$U_{ct,Fy}$=1.4 lbf	$U_{ct,My}$=1.3 in*lbf
$U_{ct,Fz}$=0.35 lbf	$U_{ct,Mz}$=9.3 in*lbf

2.5 TEST MEASUREMENTS

For each test of a simulated truck motion, there were two sets of measurements. First, the tank without any liquid was subjected to the motion. The measurements from these dry tank tests served as a baseline to assess the magnitude of the liquid loads and provided a set of data to check the rigid body model of the test setup. Next, the tank loaded half-full with water was subjected to each motion profile. The combined predictions of the rigid body simulation of the dry tank and the CFD predictions for slosh load are compared to these wet tank measurements.

For the sake of clarity, the measured and predicted force and moment components are all located in Appendix C. In all cases, the loads are resolved at the geometric center of the tank. The discussion of the comparison of the measured and predicted values is withheld until after the CFD analysis is presented in Section 3.

3. SLOSH LOAD PREDICTIONS AND DATA ANALYSIS

In this section, the fluid motion analysis of the test tank is described and the predictions for the total (tank and fluid) loads are compared to the measured loads.

3.1 CFD MODEL SETUP

The motion of the fluid in the tank was simulated with the software package, FLOW-3D® (Flow Science, Inc.). This software is a general purpose CFD analysis package that has historically been one of the best analysis tools for studying the dynamic behavior of fluids with free surfaces. This package is used widely in the aerospace industry to predict the loads on spacecraft due to the movements of liquids in fuel tanks.

This software uses a structured grid to discretize the flow domain. The FAVOR (fractional area and volume ratio) method is used to represent solid objects within the flow domain and the VOF (volume of fluid) method is used to track the free surface configuration throughout the flow domain in response to the fluid dynamics. Both of these methods were pioneered by the authors of FLOW-3D®, and the VOF techniques have been incorporated into other software packages for computing free surface flows.

3.1.1 Computational Mesh

The coordinate system for the CFD analysis was placed at the geometric center of the tank and aligned with the vehicle coordinate system (i.e., positive y-axis toward the front of the vehicle, positive z-axis upward). This coordinate system is body-fixed. The tank walls were described using the geometry primitives provided in FLOW-3D®. The ends of the tanks were defined as planes and the barrel of the tank was defined as an ellipse consistent with the design shape of the test tank. The actual test tank surface did not precisely follow the design shape, but this discrepancy was ignored.

Figure 3.1 shows the computational mesh and the modeled solid surfaces of the tank walls. The final computational mesh consisted of 32 cells along the x-axis (lateral direction), 20 cells along the y-axis (longitudinal direction), and 24 cells along the z-axis (vertical direction). This specification provided for computational cells that were almost cubes. There are 15,360 cells in the mesh; however, the cells completely blocked from the fluid by the tank wall definition are not active in the flow calculations.

No special attention was given to refining the mesh near the tank walls. Modeling the boundary layer in this situation is unnecessary because localized viscous effects are negligible in comparison to inertial effects for large-scale short-lived tank motions. Global viscous effects were accounted for under the assumption that the flow was locally laminar.

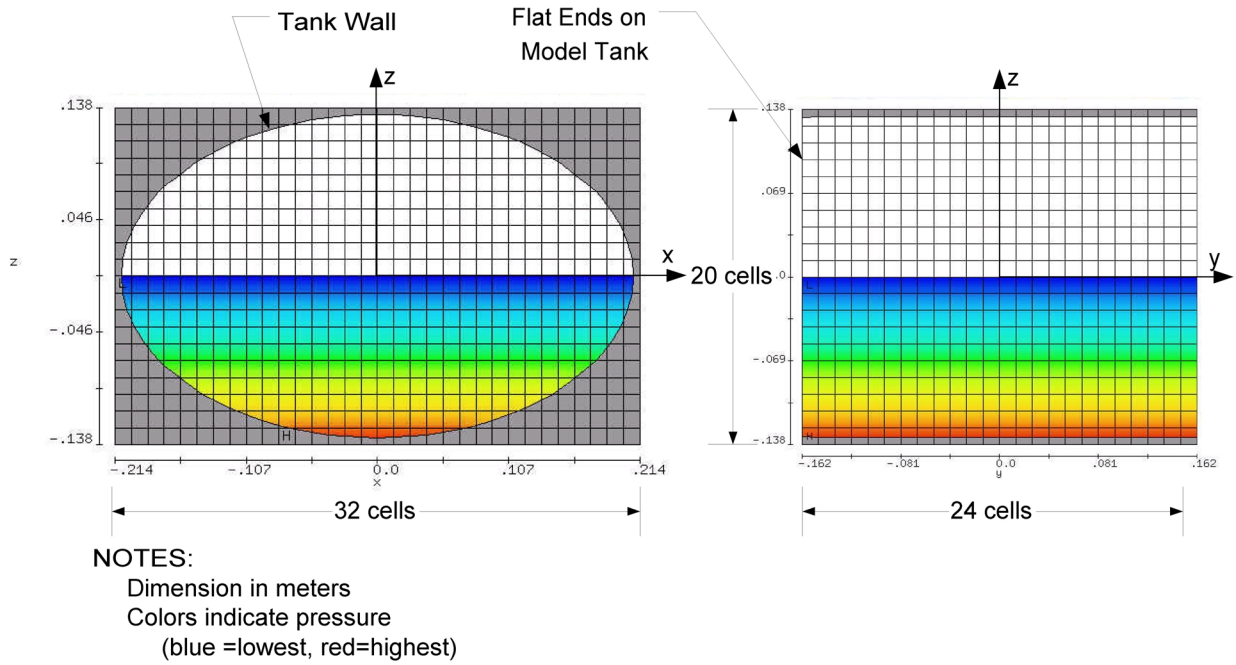

Figure 3.1. Computational Mesh Definition.

3.1.2 Fluid Properties

The test fluid was water; so the following fluid properties were specified for the CFD analysis:

Density = 62.4 lb/ft^3 (1,000 kg/m^3)

Viscosity = 6.7×10^{-4} lbm/ft·s (0.001 Pa·s)

3.1.3 Motion Description

FLOW-3D® simulates the fluid dynamic response to imposed motions by allowing the user to describe the motion of the body-fixed coordinate system within an inertial coordinate system. In the cases studied here, the motion of the body-fixed coordinate system attached to the test tank is purely by rotation about the fixed point at the front of the frame supporting the tank.

The three components of linear acceleration, angular velocity, and angular acceleration of the body-fixed system with respect to the inertial coordinate system must be defined by the user. These quantities were obtained from a dynamics analysis of the test hardware using the actual hydraulic cylinder displacement measurements to provide the driving force. FLOW-3D® uses a linear interpolation algorithm to compute the required instantaneous values from a file containing the time history of these parameters. The FLOW-3D® software internally computes the local relative kinematics of the fluid with respect to the body-fixed coordinate system (i.e., local linear and coriolis accelerations) to complete the kinematics definition. While the body-fixed coordinate system in this scenario did not have any linear motion with respect to the inertial reference, the effect of the gravitational force variations in the body-fixed system was modeled as a linear acceleration vector.

Recall that the motions used in the tests are not a precise simulation of the six degrees-of-freedom definition of the vehicle motion provided by TACOM. The motions used in these tests are only approximations of these motions within the constraints of the test setup using a fixed point at the roll center of the front axle.

3.1.4 Grid Independence Assessment

The CFD simulations were initially executed using half the grid resolution described above (*i.e.*, 16x10x12 cells for a total of 1,920 cells). There were only slight deviations in the computed fluid forces for the two levels of grid resolution. The higher resolution grid required less than about 30 minutes of computation time for the longest simulation, compared to 30 seconds of CPU time for the coarse-grid simulation. So, the higher resolution scheme was retained for all the simulations in spite of the small differences in the fine and coarse grid results.

3.2 DATA ANALYSIS

3.2.1 Measured and Predicted Loads

The time history forces and moments applied by the dry tank on the force sensors during each motion sequence were predicted by a rigid body analysis provided by Working Model 3D®. Likewise, the forces and moments applied by the fluid on the tank walls were predicted by FLOW-3D®, as described above. These predicted forces and moments were summed at the center of the tank to provide a prediction for the total loads applied to the tank supports. These predictions were then compared to the time history of the loads obtained from the data measured in the laboratory tests. The predicted and measured values of each of the force and moment components for all six motion sequences are found in the graphs of Appendix C.

3.2.2 Roll Moment Comparison

The graphs shown in Appendix C present the details of the correlation of the predicted and measured loads. These loads are defined at the center of the tank and are useful in defining the quality of the predictions. A more important parameter of interest to overall vehicle stability is the moment about the vehicle roll axis.

The roll center of the front and rear axles of the FMTV vehicle are not at the same vertical position in the vehicle coordinate system. So, the vehicle roll axis is not parallel to the ground or the vehicle coordinate system. In the scale model, the roll moment arm for the F_x component at the rear axle was specified as 13.84”. An approximation to the scaled value of the vehicle roll moment was obtained by summing the tank’s y-moment, M_y, and the transfer moment due to F_x from the measured and predicted loads at the tank center. These roll moment values are compared for each of the simulated maneuvers in Figures 3.2—3.7.

In these graphs, the response of the tank and fluid to the motion is shown for a time period starting 1-2 seconds prior to the main motion profile and lasting for 2-3 seconds after the main profile is completed. In all cases, it is seen that there is a 4-Hz oscillation present in test data before the main motion begins. This is a response to the high frequency ‘noise’ in the motion profiles provided by TACOM. Since the same motion profiles were used to drive the test hardware, the rigid body, and CFD simulations, the predicted data show the same response as the test data prior to the main motion profile.

AVTP Lane Change. The predicted and measured rear axle roll moment for the 20-mph and 40-mph lane change maneuvers are shown in Figures 3.2 and 3.3, respectively. There is good overall agreement between the predictions and measured data, but there are short-lived regions where the agreement is not good (e.g., at 4—4.2 seconds in the 20-mph lane change). The maximum roll moment in the 20-mph lane change is about 100 in-lbf, and the peak value of the 40-mph lane change is about four times greater. The plots for all of the cases, Figure 3.2 through Figure 3.7, show the roll moment of the scaled model analysis on the left axis. The right axis is the value of the roll moment if scaled up to full scale, which is a moment scale factor of 370 to 1.

During most of the motion in the 40-mph maneuver, the fluid is not adding any significant additional dynamic features to the roll moment beyond its effect as a rigid mass. This is indicated by the fact that the predictions for the dry tank alone show most of the oscillatory features that the combined predictions and the measured data show, but at a reduced magnitude. In general, the magnitude of the peak roll moments for the wet tank is approximately twice that of the dry tank. The effect of the fluid is more pronounced in the 20-mph lane change. It is seen that the moment due to the dry tank alone has a relatively smooth profile throughout this time period. The measured data and the predictions for the total load (tank plus fluid) show a significant periodic response with a frequency of a little greater than 1 Hz. This is indicative of a large fluid slosh component and it can be shown that the fluid has a slosh resonance of about 1.2 Hz (Abramson [1966]). This phenomenon is present in the 40-mph maneuver, but the magnitude is less than half that demonstrated in the 20-mph maneuver. Clearly, the 20-mph lane change excites the first mode of slosh resonance in this tank.

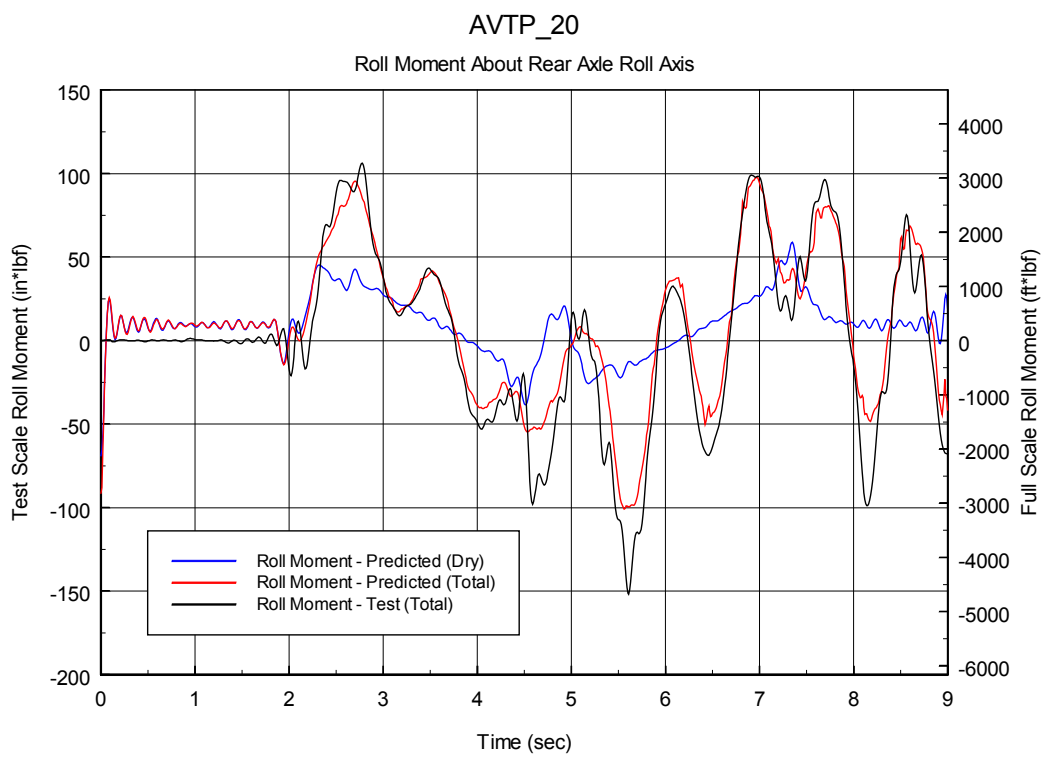

Figure 3.2. Rear Axle Roll Moment, 20-mph Lane Change.

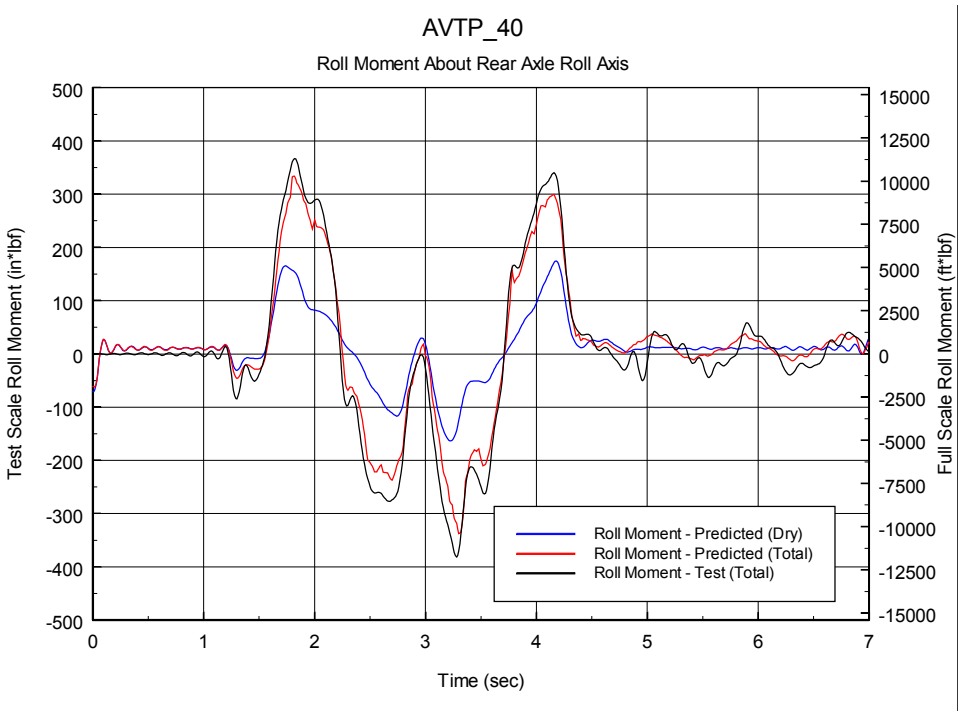

Figure 3.3. Rear Axle Roll Moment, 40-mph Lane Change.

Trapezoidal Asymmetric Bump. The predicted and measured rear axle roll moment for the 9" trapezoidal bump at 15 mph and the 12" trapezoidal bump at 10 mph maneuvers are shown in Figures 3.4 and 3.5, respectively. There is agreement between the predictions and measured data on several levels.

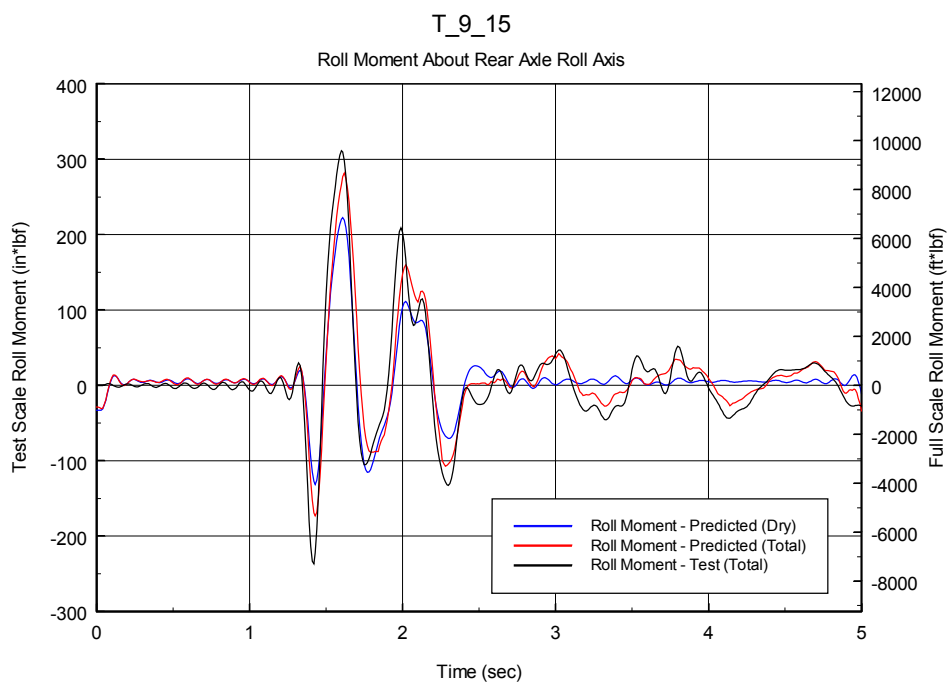

Figure 3.4. Rear Axle Roll Moment, 9" Trapezoidal Bump at 15 mph.

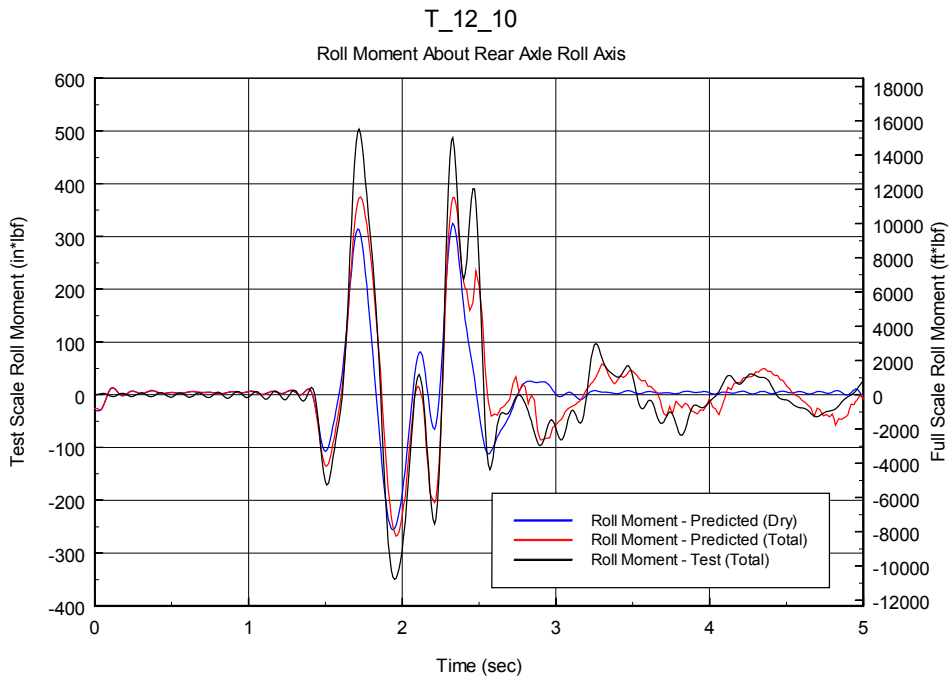

Figure 3.5. Rear Axle Roll Moment, 12" Trapezoidal Bump at 10 mph.

The match between the predictions and measurements is good in that the overall shape of the predicted roll moment closely follows the measurements. Also, the CFD predictions show several fluid-related effects that are subtle but significant.

The first of these areas is in the time period of 1.6 to 1.8 seconds for the 9" bump case. The analysis shows that the fluid amplifies the local roll moment peak beyond the effect of the dry tank alone, but that at 1.6 seconds into the test not all of the fluid is acting in phase with the tank. If all the fluid were acting in phase with the tank, the roll moment would be approximately twice that of the dry tank alone, since the fluid mass is about equal to the tank mass in the scale model. This is also the reason that the total roll moment magnitude at the time near 1.8 seconds is <u>less</u> than that predicted for the dry tank alone. A portion of the fluid is out of phase with the tank motion and acts to <u>reduce</u> the roll moment in agreement with the measured data.

Finally, the fluid acts to provide for a double peak in the roll moment at a time of 2.5 seconds in the case of the 12" bump. The magnitude of the second of these peaks is not exactly matched by the predictions, but the analysis shows that the second peak is due solely to the fluid, as predicted by the CFD simulation.

Half-Round Symmetric Bump. The predicted and measured rear axle roll moment for the 9" half-round bump at 10 mph and the 12" half-round bump at 5 mph maneuvers are shown in Figures 3.6 and 3.7, respectively. The agreement between the predictions and measured data for the half round bump simulations is not as good as for the other two maneuvers. In the case of the 12" bump, the agreement is poor after about 3 seconds. This time period is after the main motion profile is over and the predictions show a much more severe roll moment oscillation than the measured data. This is due to some response predicted by the CFD simulation that is not present in the test data.

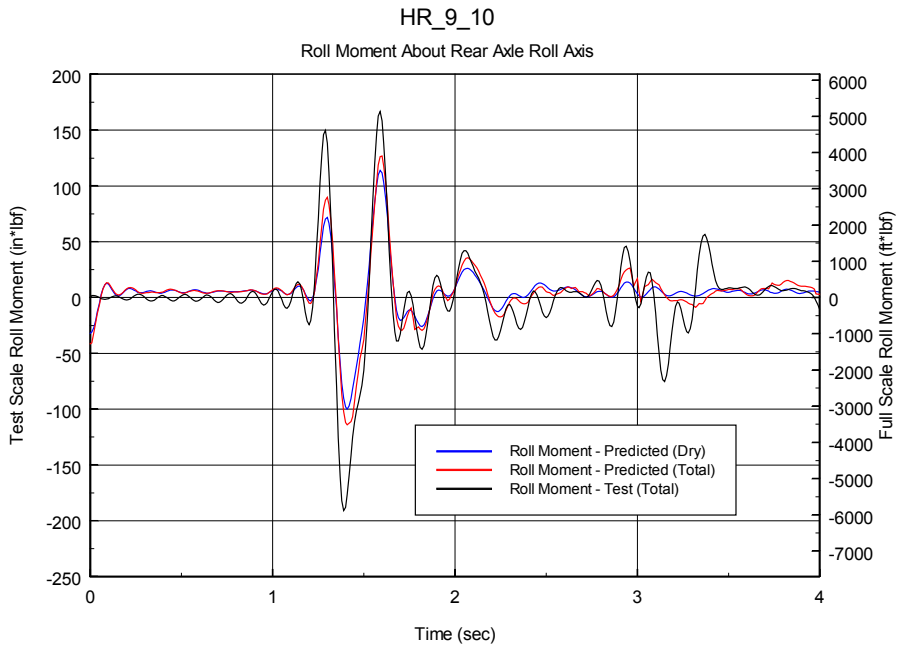

Figure 3.6. Rear Axle Roll Moment, 9" Half Round Bump at 10 mph.

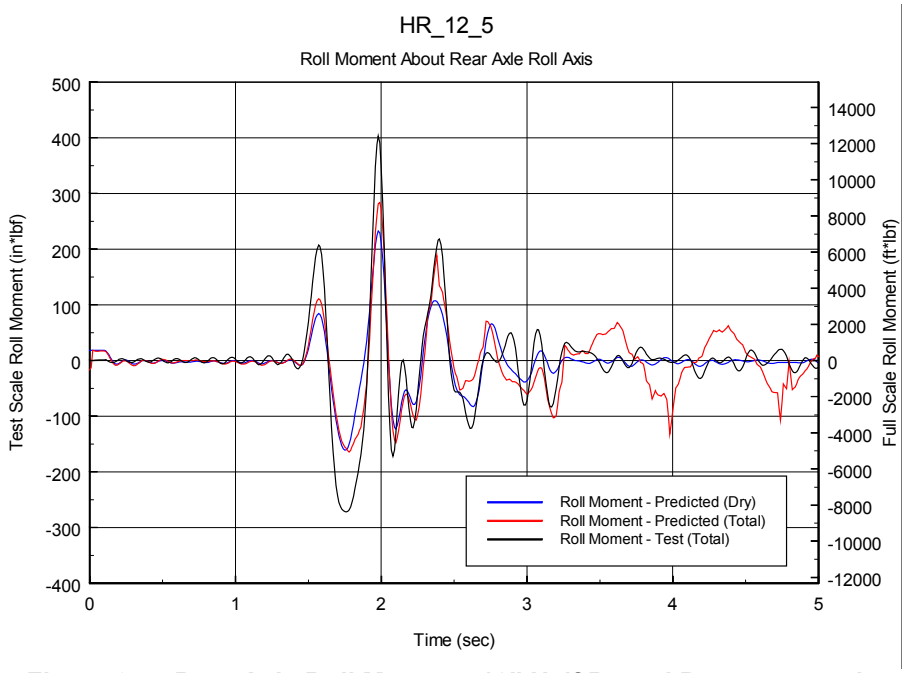

Figure 3.7. Rear Axle Roll Moment, 12" Half Round Bump at 5 mph.

This is a symmetric bump that should, theoretically, be felt by both sides of the vehicle equally. The roll moment, however, is shown to be only slightly less than in the case of the trapezoidal bump. The motion profiles provided by TACOM, however, for the left and right positions above the rear axle show a slightly asymmetric behavior. This asymmetry is reflected in the predictions and the test data presented here.

There are differences between the predicted and measured roll moments for the dry tank alone that are a large portion of the deviations in the corresponding total roll moment values shown in Figures 3.6 and 3.7. The cause of this deviation is not readily understandable, given the quality of agreement in the other two motions and the fact that the modeling approach is identical for all cases.

3.2.3 Fluid Motion Comparisons

The fluid motion, as observed by two different cameras, was recorded simultaneously on videotape for each of the six simulated maneuvers. One camera was placed on the tank looking along the negative y-axis direction into the forward tank flange. The second camera was placed such that it viewed the left side of the tank looking along the positive x-axis.

Likewise, the fluid configuration predicted by FLOW-3D® was saved at 0.1-second intervals for comparison to the video recordings. Overall, the simulated fluid motions closely follow the actual fluid motions. Two examples of this motion are shown in Figure 3.8 for the 20-mph lane change and Figure 3.9 for the 12" trapezoidal bump at 10 mph. Both these figures show selected still images captured from the videotape and the FLOW-3D® animation.

The measured and predicted fluid configurations are compared here only for the camera looking back along the y-axis. In both figures, the specified time is with respect to the start of the main motion.

During the 20-mph lane change, the fluid demonstrates large amplitude sloshing and small waves roll across the surface, but the fluid does not splash. This is almost linear sloshing and the motions are the most benign of those tested. There is about a 2.0-second shift between the data presented in Figure 3.2 and the time values in Figure 3.8. So, in Figures 3.8a and 3.8b, the fluid configuration corresponds to the roll moment peak at about 2.7 seconds in Figure 3.2, and in Figures 3.8c and 3.8d, the fluid configuration corresponds to the roll moment peak at about 8.2 seconds in Figure 3.2. The predicted fluid motion compares well with the recorded motion. Note that the small surface wave near the right side of Figure 3.8c is simulated in Figure 3.8d.

The fluid response to the 12" trapezoidal bump was one of the most violent for the cases studied here. The sequences presented in Figure 3.9 show that the predicted fluid configuration agrees well with the recorded fluid motion for this maneuver. First, the fluid wave height against the tank wall at a time of about 0.4 seconds matches the recorded fluid shape in this region. There is, however, a moderate inflection in the surface that is not as strongly demonstrated in the recorded fluid shape. Next, the large cresting wave that is breaking over the main fluid surface at a time of 0.8 seconds is closely matched by the CFD predictions. Finally, at a time of 1.6 seconds, the fluid is stacked against the front left corner of the tank (the right corner in this image looking backwards) in the video recording. This is predicted at a slightly later time by the CFD prediction.

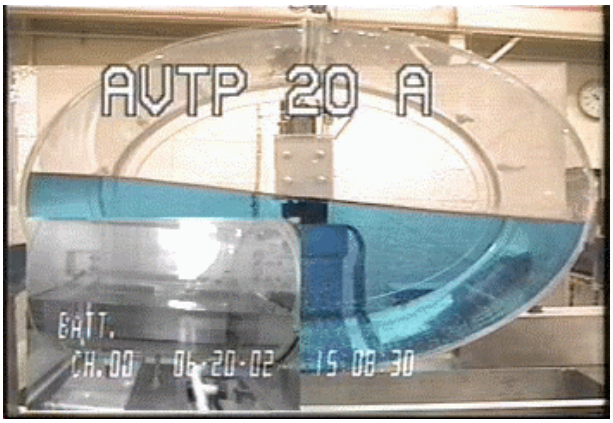

a. Test at 0.70 seconds.

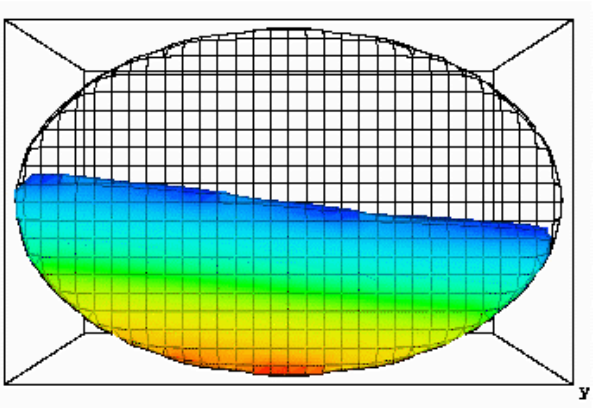

b. CFD Simulation at 0.60 seconds.

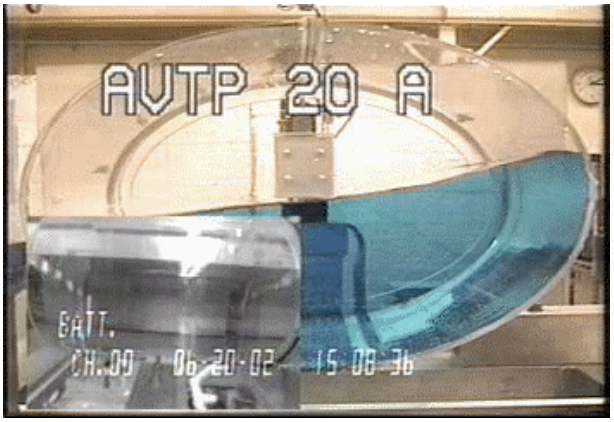

c. Test at 6.17 seconds.

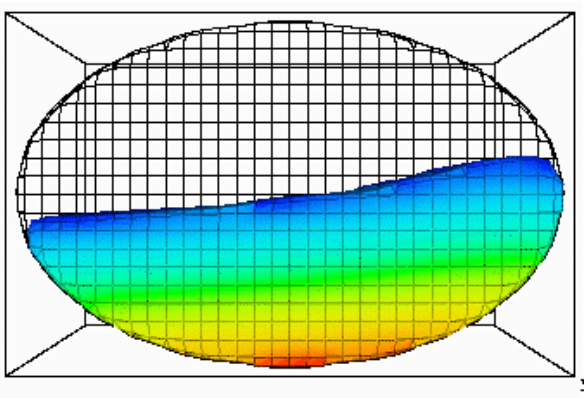

d. CFD Simulation at 6.20 seconds.

Figure 3.8. Fluid Configuration for 20-mph Lane Change.
The viewpoint in these images is from the front of the vehicle looking in the negative y-direction. The inset in the video image is viewing the tank from the left side of the vehicle.

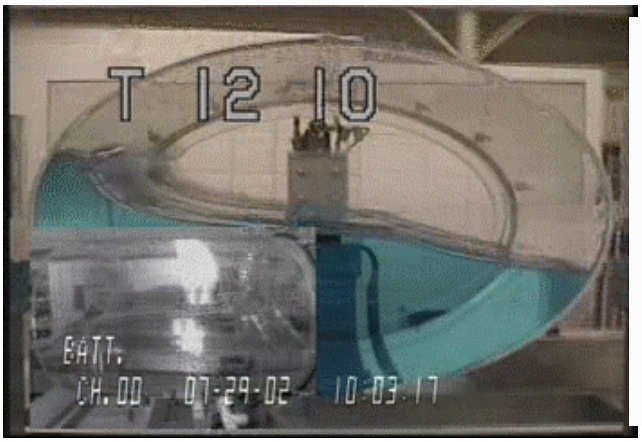

a. Test at 0.43 seconds.

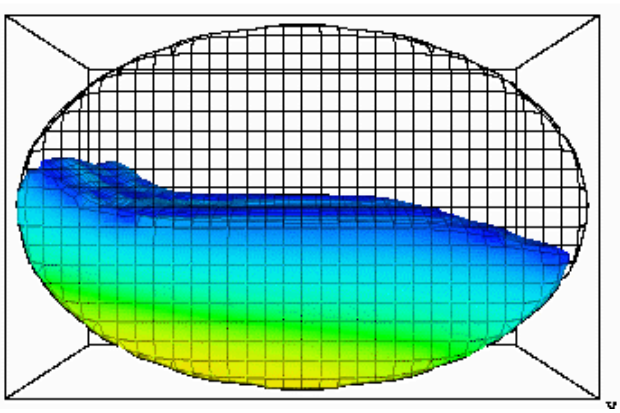

b. CFD Simulation at 0.40 seconds.

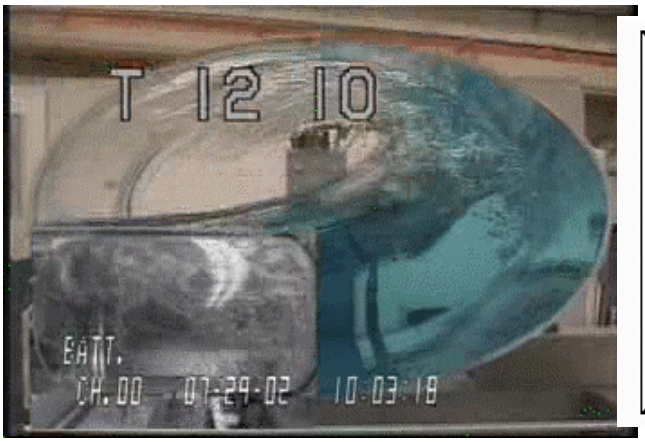

c. Test at 0.80 seconds.

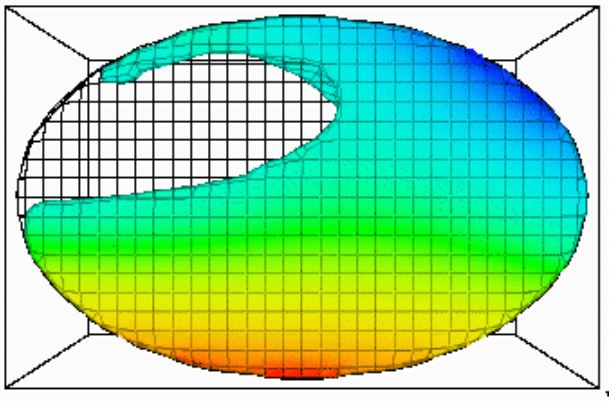

d. CFD Simulation at 0.90 seconds.

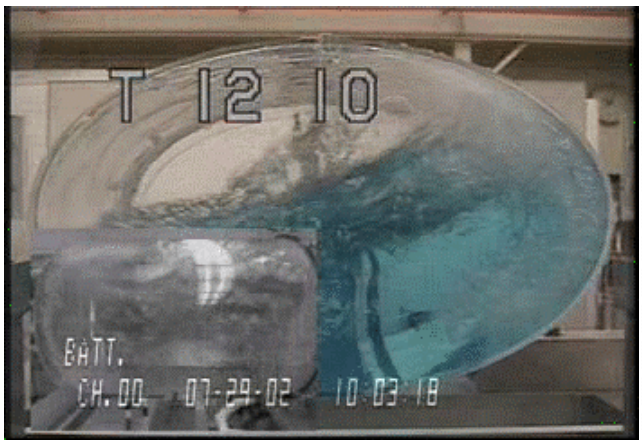

e. Test at 1.53 seconds.

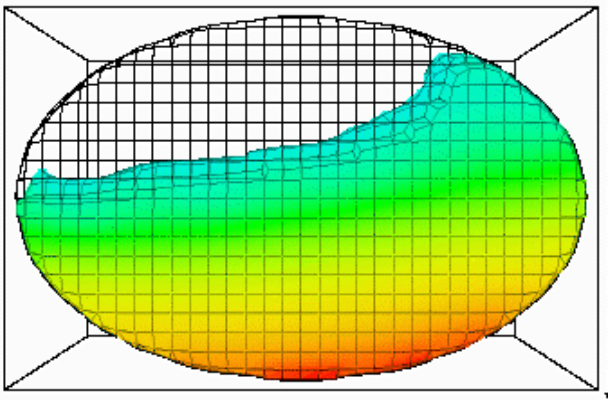

f. CFD Simulation at 1.60 seconds.

Figure 3.9. Fluid Configuration for 12" Trapezoidal Bump at 10 mph.
The viewpoint in these images is from the front of the vehicle looking in the negative y-direction. The inset in the video image is viewing the tank from the left side of the vehicle.

4. CONCLUSIONS AND RECOMMENDATIONS

In this project, a scale model of a water transport tank attached to an FMTV vehicle was fabricated for testing the response of the liquid to six different vehicle maneuvers. The test tank was mounted to a frame that was allowed to rotate about three axes at a point that corresponded to the vehicle's front axle roll center. The test tank was fabricated of clear acrylic and was a 1/4.4 scale of an actual tank. The frame was supported by two hydraulic cylinders that corresponded to positions on either side of the vehicle at the elevation of the rear axle roll center. The motion of the independent hydraulic cylinders was prescribed in such a way that the frame motion, within the constraints of the test setup, approximated the following six maneuvers:

- AVTP Lane Change at 20 mph
- AVTP Lane Change at 40 mph
- 12" Half-Round Symmetric Bump at 5 mph
- 9" Half-Round Symmetric Bump at 10 mph
- 12" Trapezoidal Asymmetric Bump at 10 mph
- 9" Trapezoidal Asymmetric Bump at 15 mph

The objective of these tests was to provide a set of data with which to assess the validity of a computational fluid dynamics approach to the analysis of the fluid motions and the loads imparted by the fluid on the vehicle. The CFD analysis was conducted with the commercially available software package, FLOW-3D™. A relatively coarse mesh of about 15,000 cells was used in the analysis that was shown to yield a grid-independent simulation. With this flow domain specification, each of these simulations was completed in less than about 15 minutes on a dual-processor workstation with each processor operating at 1 GHz.

The three components of force and three components of the moment at the tank center were the primary data resulting from the laboratory tests. The measurements represented the load (force and moment) required to move the tank and the fluid through the prescribed motions. Also, the fluid motion was recorded by two video cameras; one looking left at the front tank bulkhead and one looking right at the left tank wall.

The predicted and measured loads are compared for all force and moment components, but the parameter of most importance is considered to be the moment about the vehicle roll axis. From that standpoint, there is good correlation between the predicted and measured roll moment. Some details of the response at frequencies greater than about 2 Hz are not in total agreement. Also, the predicted peak roll moment is as great as 30% different than the measured value, but the main features of the tank and liquid dynamic behavior are closely predicted. The discrepancy between the measured and predicted roll moment peaks varies according to the harshness of the maneuver. The error is smallest for the lane changes and is greatest for the half-round bumps. This agreement is also obtained in comparing the recorded fluid motion with the animation of the CFD predictions for the fluid configuration during the maneuvers.

There were discrepancies between the measured loads for the dry tank and the loads predicted by the rigid body model of the tank and test frame. At some times in the analysis, these dry-tank deviations were a large part of the overall deviation between the measured and predicted loads for the wet tank. The sources of the discrepancies in the dry-tank load predictions are thought to be a result of neglecting the stiffness of the structures and inaccuracies in modeling the test fixture joints. The discrepancy between the predicted and measured loads is

reduced appreciably if the fluid-related loads computed by the CFD analysis are summed with the measured loads for the dry tank. This combination of measured and predicted loads was not presented in this report in order to preserve a clear distinction between the experiment results and the analytical results.

Overall, the results presented here show that CFD can successfully be applied to the study of fluid motions and the fluid-structure interactions in truck-mounted water transport tanks. In some cases, the fluid sloshing effects are significant. As has been demonstrated in some accidents, the vehicle dynamics and fluid dynamics can be strongly coupled. Given the rapid turnaround time for the CFD simulations presented here, the outlook is encouraging for coupling a vehicle rigid body dynamics analysis to a fluid dynamics analysis for a high fidelity simulation of the complete vehicle response to maneuvers.

Based on the success demonstrated here, it is recommended that work proceed on the coupling of a CFD model of tank fluid motions with vehicle dynamics models of Army trucks. Preliminary discussion with the vendors of FLOW-3D® (Flow Science, Inc.) and FLUENT® (Fluent, Inc.) indicate that either of these packages can be adapted to communicate with other software in this way. FLOW-3D® was used in the current project and performed well in all respects for this uncoupled analysis. Nevertheless, each of these codes should be more thoroughly assessed in order to make the proper choice from the standpoint of ease of use, accuracy, and computational speed when coupled with the vehicle dynamics modeling software.

5. REFERENCES

Abramson, H.N. [1966], ***The Dynamic Behavior of Liquids in Moving Containers***, NASA SP-106.

Flow Science, Inc. [2001], ***FLOW-3D®,*** Version 8.0.1, Santa Fe, New Mexico.

Working Model, Inc. [1997], ***Working Model 3D®***, Version 2.0, San Mateo, California.

Coleman, H.W., Steele, W.G. [1989], ***Experimentation and Uncertainty Analysis for Engineers,*** John Wiley and Sons, New York, 1989.

APPENDIX A: ROLL APPROXIMATION FOR LANE CHANGE MANEUVERS

For each lane change maneuver, the dominant acceleration - lateral (x-direction) acceleration - was simulated with a pure rolling motion. The roll angle profile was developed such that the sum of the body force acceleration due to tilting the tank in the gravity field and the tangential acceleration due to the rolling motion would match average lateral acceleration from the FMTV truck simulation. The objective here was not to provide a high fidelity simulation to all six degrees of freedom for the actual maneuver. Rather, the purpose was to provide an approximation to the actual tank motion to serve as a basis for assessing the validity of the CFD analysis of the fluid motion and fluid-structure loads. In particular, the role angle profile was found by solving the following differential equation:

$$R\ddot{\theta} + \beta\dot{\theta} + g\sin(\theta) = a_x(t) \qquad \text{(A.1)}$$

where, $a_x(t)$ = average lateral acceleration from FMTV truck simulation
θ, $\dot{\theta}$, $\ddot{\theta}$ = roll angle, angular velocity, angular acceleration
g = acceleration due to gravity
β = "damping" coefficient
R = distance from tank center to roll center

Figure A.1 shows a sketch of the test rig in a pure rolling motion. A fictitious term ($\beta\dot{\theta}$) corresponding to damping in a simple mass-spring-damper system was added in order to allow the solution to converge. The value of the "damping" coefficient, β, was adjusted until good agreement between the shape of the roll angle profile and the average lateral acceleration profile was observed.

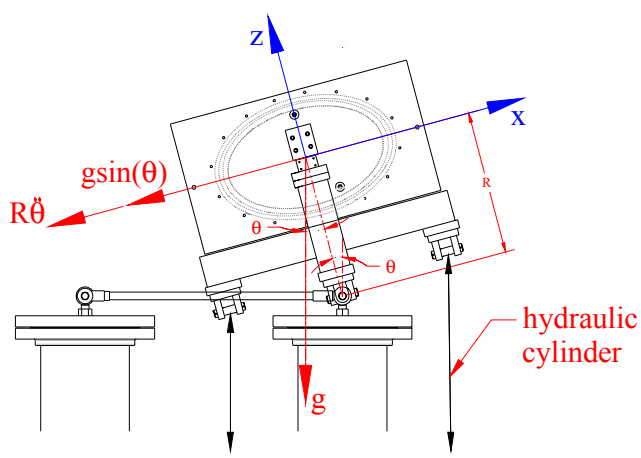

Figure A.1. Lane Change Roll Profile Development (View From Rear of Vehicle).
The roll angle profile was developed such that the sum of the body force acceleration due to tilting the tank in the gravity field [gsin(θ)] and the tangential acceleration due to the rolling motion [$R\ddot{\theta}$] would match average lateral acceleration from the FMTV truck simulation.

Equation (A.1) was solved as the following system of first order differential equations using an Euler numerical integration technique.

$$\frac{d\theta}{dt} = \dot{\theta} \tag{A.2}$$

$$\frac{d\dot{\theta}}{dt} = \frac{a_x(t) - g\sin(\theta) - \beta\dot{\theta}}{R} \tag{A.3}$$

The roll angle profile solution from Eqs. (A.2) and (A.3) was converted to hydraulic cylinder displacement time histories used as the command input to the servo control system to execute the lane change maneuvers. Comparisons between the lateral force measured during the dry-tank testing and the lateral force calculated as the dry tank mass (32.5 lb) times the scaled average lateral acceleration provided by TACOM are given in Figures A.2 and A.3 for the 20-mph and 40-mph lane change maneuvers, respectively. In each case, the roll angle profile solution yielded motion for which the measured lateral force profile closely matched the shape of the target, calculated lateral force profile.

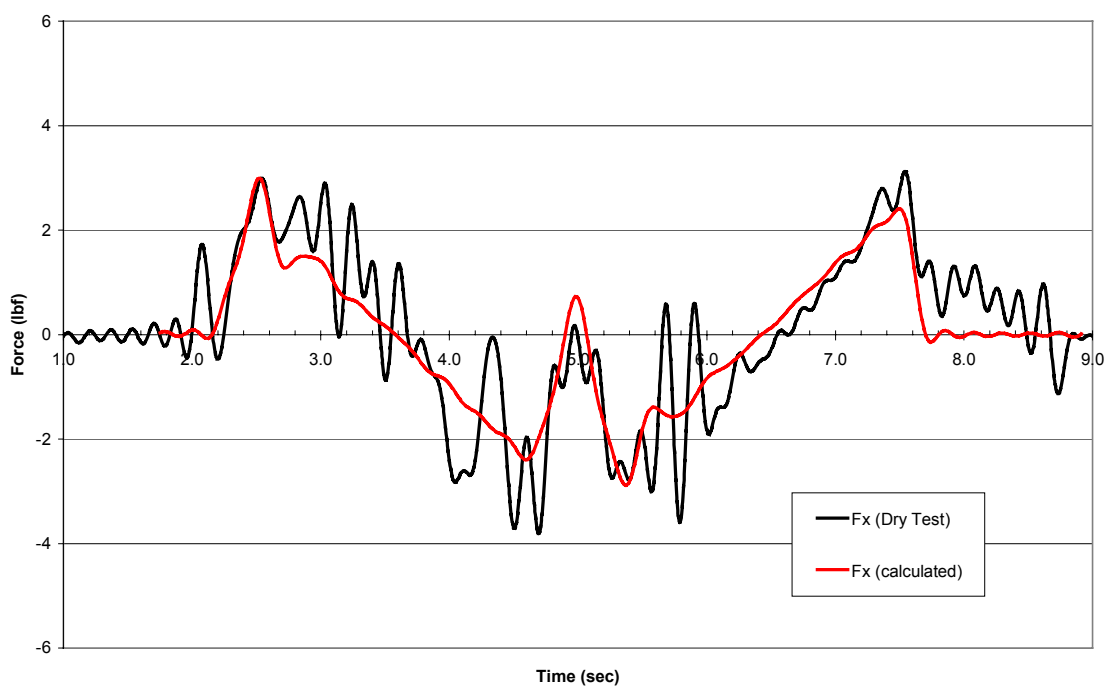

Figure A.2. 20-mph Lane Change (AVTP_20) Lateral (x-direction) Force Comparison. *The measured lateral force profile closely matched the shape of the target, calculated lateral force profile. The roughness of the measured lateral force profile was caused by friction in the hydraulic cylinders, which are actuated relatively slowly in this maneuver.*

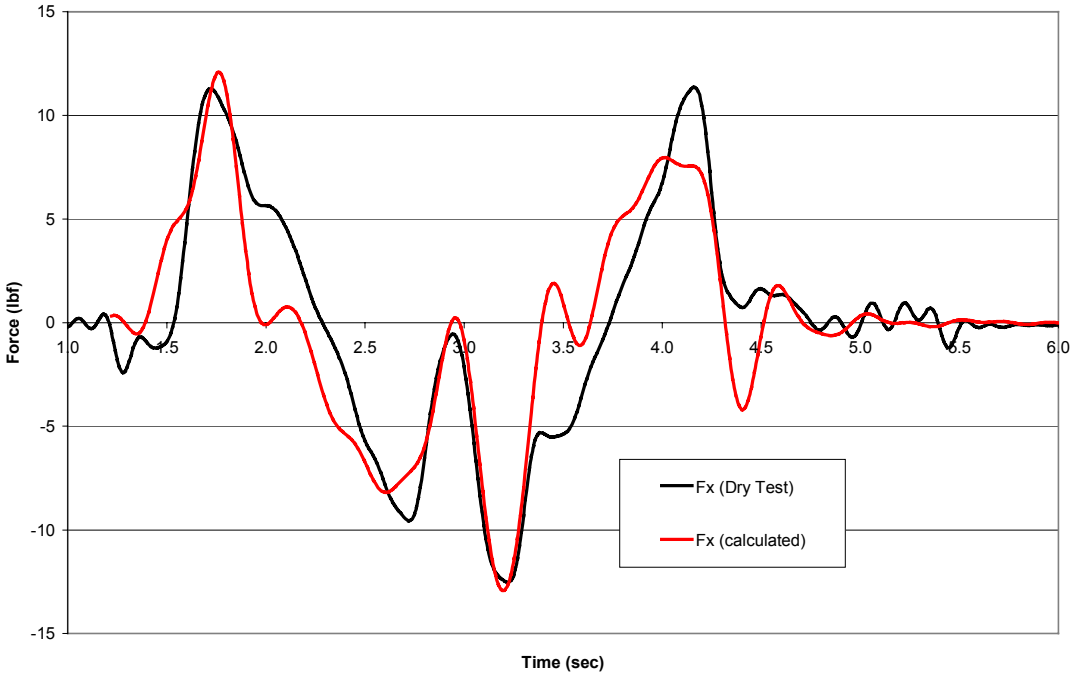

Figure A.3. 40-mph Lane Change (AVTP_40) Lateral (x-direction) Force Comparison.
The measured lateral force profile matched the shape of the target, calculated lateral force profile.

APPENDIX B: UNCERTAINTY ANALYSIS

There are many sources of error or uncertainty in the measurement and processing of the force sensor voltage signals in order to arrive at the three net force and moment components described in this report. Among the sources of error are hysteresis and stability of the sensor elements, random errors in the electrical and digital instrumentation, linearity in converting the voltage signals to engineering units, and crosstalk between the sensor components. During the sensor calibration procedures, it was discovered that curve fit errors (i.e., engineering unit conversion linearity) and crosstalk were, by far, the dominant sources of uncertainty in the measurement of the loads on the sensor assembly.

For the purposes of this discussion, the term 'crosstalk' refers to the voltage signal that is measured on force sensors when a load is applied for which there should ideally be no signal present. For example, an output from the x-direction component of the multi-axis force sensor when only a y-direction load is applied is considered a crosstalk signal. This can be a result of inherent crosstalk in the multi-axis sensor package installation errors, or the support structure deforming under load to change the direction of the sensor axis.

CURVE FIT UNCERTAINTY

The force sensor calibrations showed that the response of each of the nine sensors was not precisely linear with respect to the applied force and moment components. A linear expression for the engineering unit conversion, however, was maintained in the data processing procedure. The magnitude of this source of error is estimated as follows.

It was shown in Section 2 that the output of the nine force sensors could be combined in different ways so that the applied load is directly proportional primarily to a particular sensor output combination. The other terms are considered to be the crosstalk terms. This is expressed mathematically in Eq. 2.4. Each of the 54 sensitivity terms contributing to the 6x6 matrix, **K** in Eq. 2.4 is actually a line fit through a series of voltage values corresponding to the sensors' responses to the applied loads. The sensor voltage variance about this line is used to determine the portion of the possible variance of the applied load due to a single sensor's variance. For example, the variance in the x-component of force due to the voltage variance of the x-component of sensor #1 is

$$Fx_{x1+} = \left[\mathbf{K}^{-1}\right]_x V'_{x1+} \tag{B.1}$$

where $[\mathbf{K}^{-1}]$ is a single row of the inverse sensitivity matrix (see Eq. 2.4) which is used to compute the x-component of the net applied force. V'_{x1+} is the voltage combination vector in which the x-direction output of sensor #1 is evaluated at its largest positive deviation from the curve fit for that sensor and all other voltages remain at their nominal levels. This process is repeated for the pairs of maximum and minimum deviations for each of the nine sensors for this particular load component. This results in 18 samples of a load pertaining to each individual voltage variance possibility for the calculation of the F_x component. The distribution of the samples provides an estimate of the uncertainty (see Coleman and Steele [1989]) due to curve fit errors for that single load component,

$$U_{cf,Fx} = t\sigma_{Fx} \tag{B.2}$$

where $U_{cf,Fx}$ is the combined uncertainty in the F_x load component due to all curve fit errors and σ_{Fx} is the standard deviation for the entire sample of eighteen 18 F_x values indicated in Eq. B.1. The term, t, is the value for the two-tailed Student's t-distribution corresponding to 17 degrees of freedom at the 95% confidence level, namely, t=2.11.

This entire process is repeated for each of the six load components (three forces and three moments). The results are as follows

$U_{cf,Fx}$=2.3 lbf	$U_{cf,Mx}$=6.1 in*lbf
$U_{cf,Fy}$=4.5 lbf	$U_{cf,My}$=2.0 in*lbf
$U_{cf,Fz}$=0.3 lbf	$U_{cf,Mz}$=34 in*lbf

These uncertainty values are expressed as magnitudes of force and moment, since they are constant over the entire load range. That is, these uncertainty values do not diminish as the loads go to zero.

CROSSTALK UNCERTAINTY

The sensor crosstalk elimination process is described in Section 2. This process is based on the nominal values of the sensor sensitivities and does not eliminate all of the crosstalk for all load levels and load combinations. The crosstalk uncertainty is an expression of the residual crosstalk that remains when the crosstalk elimination process is performed. The crosstalk uncertainty is not a fixed value and can only be estimated from an example set of test data.

First, a matrix of crosstalk uncertainty factors is developed using the maximum loads applied during the calibration procedure. These factors essentially form another type of sensitivity matrix whose members are approximate partial derivatives of the crosstalk in each load component with respect to computed values of the other components. The diagonal of this matrix is set to zero,

$$\mathbf{C} = \begin{bmatrix} 0 & \frac{\delta F_x}{\delta F_y} & \frac{\delta F_x}{\delta F_z} & \frac{\delta F_x}{\delta M_x} & \frac{\delta F_x}{\delta M_y} & \frac{\delta F_x}{\delta M_z} \\ \frac{\delta F_y}{\delta F_x} & 0 & \frac{\delta F_y}{\delta F_z} & \frac{\delta F_y}{\delta M_x} & \frac{\delta F_y}{\delta M_y} & \frac{\delta F_y}{\delta M_z} \\ \frac{\delta F_z}{\delta F_x} & \frac{\delta F_z}{\delta F_y} & 0 & \frac{\delta F_z}{\delta M_x} & \frac{\delta F_z}{\delta M_y} & \frac{\delta F_z}{\delta M_z} \\ \frac{\delta M_x}{\delta F_x} & \frac{\delta M_x}{\delta F_y} & \frac{\delta M_x}{\delta F_z} & 0 & \frac{\delta M_x}{\delta M_y} & \frac{\delta M_x}{\delta M_z} \\ \frac{\delta M_y}{\delta F_x} & \frac{\delta M_y}{\delta F_y} & \frac{\delta M_y}{\delta F_z} & \frac{\delta M_y}{\delta M_x} & 0 & \frac{\delta M_y}{\delta M_z} \\ \frac{\delta M_z}{\delta F_x} & \frac{\delta M_z}{\delta F_y} & \frac{\delta M_z}{\delta F_z} & \frac{\delta M_z}{\delta M_x} & \frac{\delta M_z}{\delta M_y} & 0 \end{bmatrix} \tag{B.3}$$

The numerator in each term is residual crosstalk in each component when only the load specified in the denominator is considered. The matrix of crosstalk uncertainty factors [**C**] is used to compute the residual crosstalk for each load combination at each time in the set of measured data,

$$\mathbf{U}_{\mathbf{ct}}(t) = \mathbf{C}\begin{bmatrix} F_x(t) \\ F_y(t) \\ F_z(t) \\ M_x(t) \\ M_y(t) \\ M_z(t) \end{bmatrix} \tag{B.4}$$

As expected, the crosstalk uncertainty values vary with the magnitude of the applied loads. Using the data for the 9" trapezoidal asymmetric bump (T_9_15) as an example case shows that there is, likewise, no fixed value for the relative crosstalk uncertainty. The following <u>maximum</u> values, however, are obtained

$$\begin{aligned} &U_{ct,Fx}=0.48 \text{ lbf} && U_{ct,Mx}=1.4 \text{ in*lbf} \\ &U_{ct,Fy}=1.4 \text{ lbf} && U_{ct,My}=1.3 \text{ in*lbf} \\ &U_{ct,Fz}=0.35 \text{ lbf} && U_{ct,Mz}=9.3 \text{ in*lbf} \end{aligned} \tag{B.5}$$

APPENDIX C: MEASURED AND PREDICTED TANK LOADS

This appendix contains a graphical presentation of both the measured and predicted loads for the scale model of the TULD tank in response to simulated motion profiles. The motion profiles prescribed for these tests were adapted from the simulation results provided by TACOM for a full scale FMTV vehicle executing the six maneuvers listed in the following table.

TEST DATA CATALOG

Maneuver/Obstacle	Speed (mph)	Test Code
AVTP Lane Change	20	AVTP_20
AVTP Lane Change	40	AVTP_40
9" Symmetric Half-Round Bump	10	HR_9_10
12 "Symmetric Half-Round Bump	5	HR_12_5
9" Asymmetric Trapezoidal Bump	15	T_9_15
12" Asymmetric Trapezoidal Bump	10	T_12_10

The test codes listed in the Test Data Catalog above are an index for identifying the maneuver being described in the graphs in this appendix. Some comments about the results are provided to note the important features of the measured and predicted loads for the simulated maneuvers.

AVTP LANE CHANGE

The most significant aspect of the lane change maneuver is the acceleration along the x-axis (lateral) direction experienced by the vehicle as it makes turns. As such, the lane change maneuvers were approximated in these tests by rolling the test tank about the y-axis as described in Appendix A. The combination of rotational acceleration and gravity provides the necessary simulation of the lateral centrifugal acceleration of the actual vehicle.

Given this scenario, the only significant loads in the dataset for this motion are F_x and M_y. The other load components are expected to be negligible with respect to transient behavior and the measured data reflect this. There is an apparent signal recorded for the M_z component, but the magnitude of this parameter is less than the uncertainty estimate described in Appendix B. So, the M_z data shown for this maneuver are not valid.

The predicted value for F_x agrees very well with the measured data for the 20-mph maneuver and is in slightly lesser agreement for the 40-mph maneuver. The fluid slosh effect is clearly evident at both speeds by comparing the force profile of the empty dry tank to that of the combined tank and liquid. The peak value of M_y is under-predicted by about 20% in each case, but the dynamics of the fluid sloshing behavior are observed in this parameter as well.

ASYMMETRIC TRAPEZOIDAL BUMP

This motion should present significant levels in all six load components, except for M_z. This is demonstrated in the force and moment profiles for this maneuver.

There is a maximum of about 30% difference between the measured and predicted peak values for F_x during the main part of the motion, but the relatively low-level slosh-induced F_x oscillations are closely predicted. The F_y values are about half those of F_x and the deviation between the predicted and measured values is correspondingly greater. Also, post-motion sloshing effect on F_y behavior is overpredicted. Conversely, the F_z profile is accurately predicted by the analysis during the post-motion sloshing. The level of agreement between the measured and predicted values for values of M_x and M_y show a similar trend, except that the post-motion moments due to sloshing are more accurately predicted than the forces.

SYMMETRIC HALF-ROUND BUMP

Ideally, this motion should affect each side of the vehicle equally, and it is expected that the primary loads experienced by the tank should be F_y, M_x, and F_z dominated by its gravitational component. In fact, the simulated motions of the left and right sides of the vehicle provided by TACOM show a slight asymmetry. This asymmetry is reflected in there being a substantial transient response in F_x.

For the main part of the motion, there is up to a 50% difference between the peak values of the measured and predicted quantities of F_x and F_y, and up to about a 30% difference in the corresponding peak values for F_z. There is a conflicting level of agreement in the post-motion sloshing behavior. The M_x values are accurately predicted, but there is a significant deviation in the F_y values in the post-motion sloshing. The reasons for this discrepancy are not clear at this time.

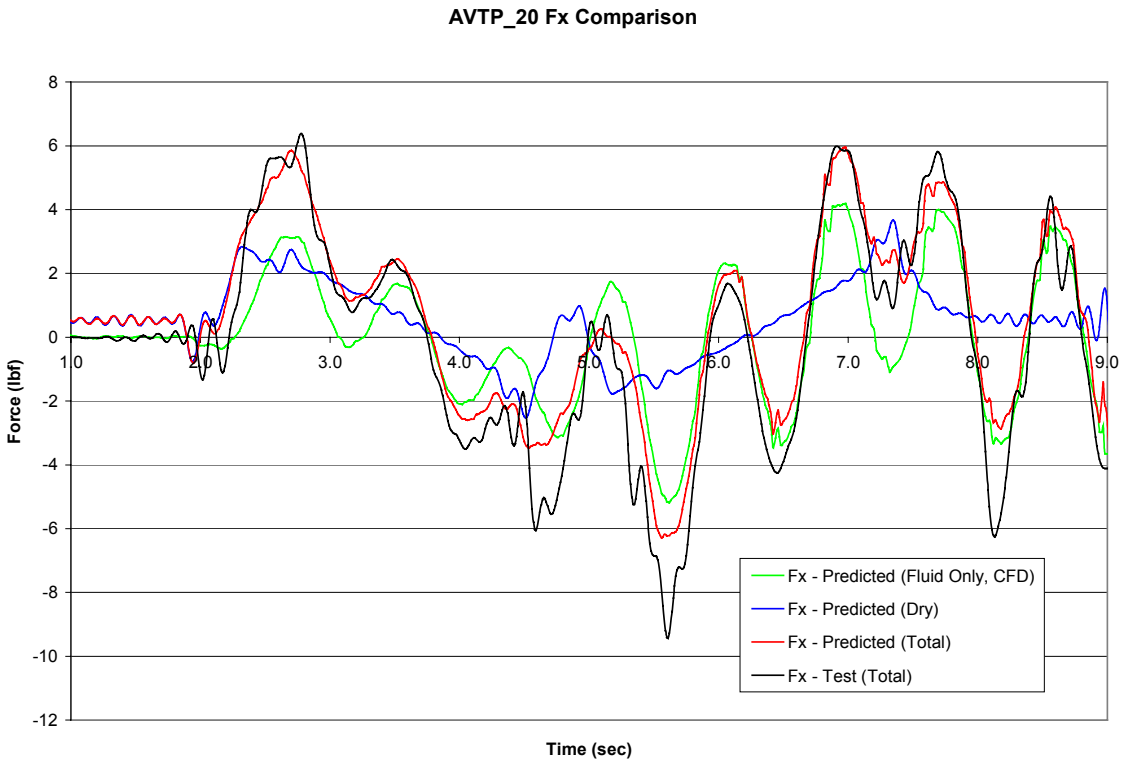
AVTP_20 Fx Comparison
Force (lbf)
Time (sec)
8
6
4
2
0
-2
-4
-6
-8
-10
-12
1.0
2.0
3.0
4.0
5.0
6.0
7.0
8.0
9.0
Fx - Predicted (Fluid Only, CFD)
Fx - Predicted (Dry)
Fx - Predicted (Total)
Fx - Test (Total)

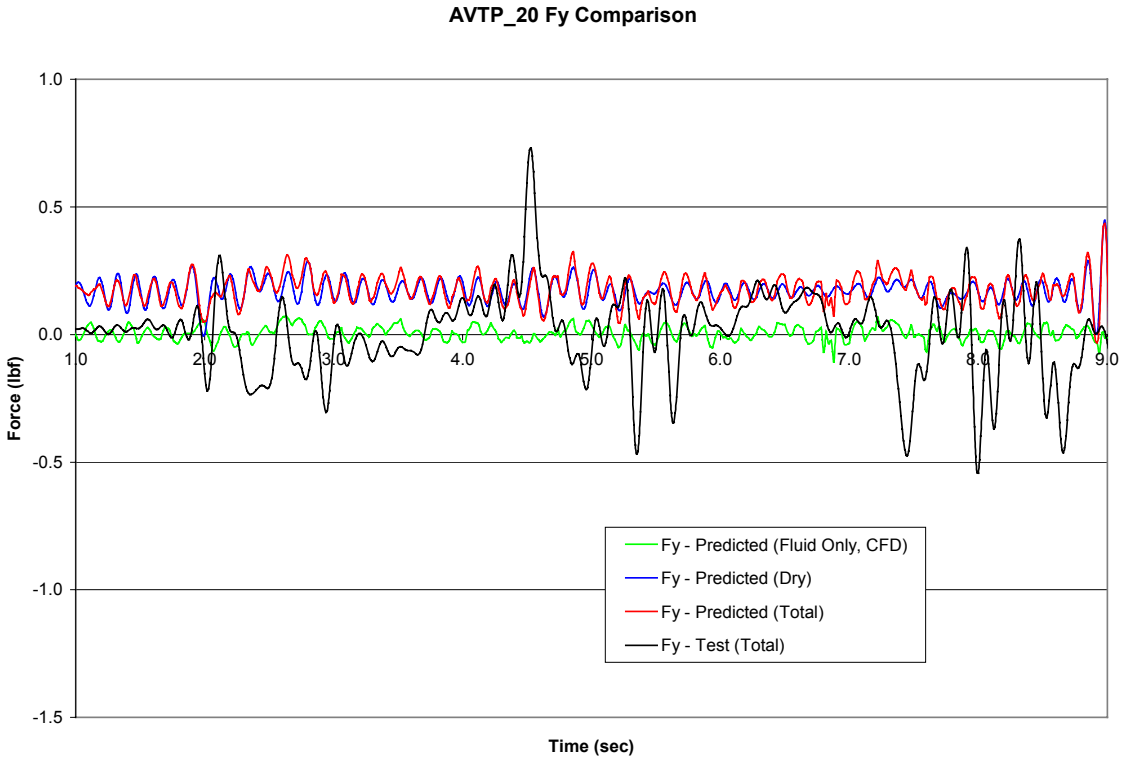
AVTP_20 Fy Comparison
Force (lbf)
Time (sec)
1.0
0.5
0.0
-0.5
-1.0
-1.5
1.0
2.0
3.0
4.0
5.0
6.0
7.0
8.0
9.0
Fy - Predicted (Fluid Only, CFD)
Fy - Predicted (Dry)
Fy - Predicted (Total)
Fy - Test (Total)

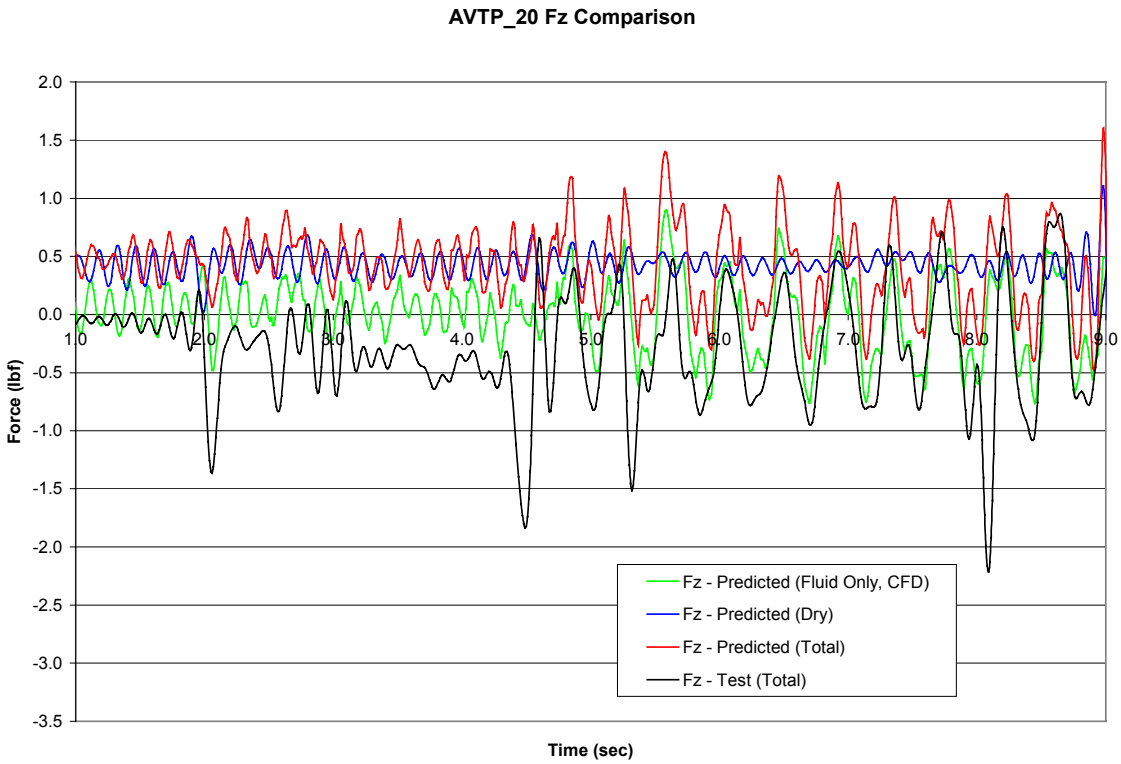
AVTP_20 Fz Comparison
Force (lbf)
Time (sec)
Fz - Predicted (Fluid Only, CFD)
Fz - Predicted (Dry)
Fz - Predicted (Total)
Fz - Test (Total)

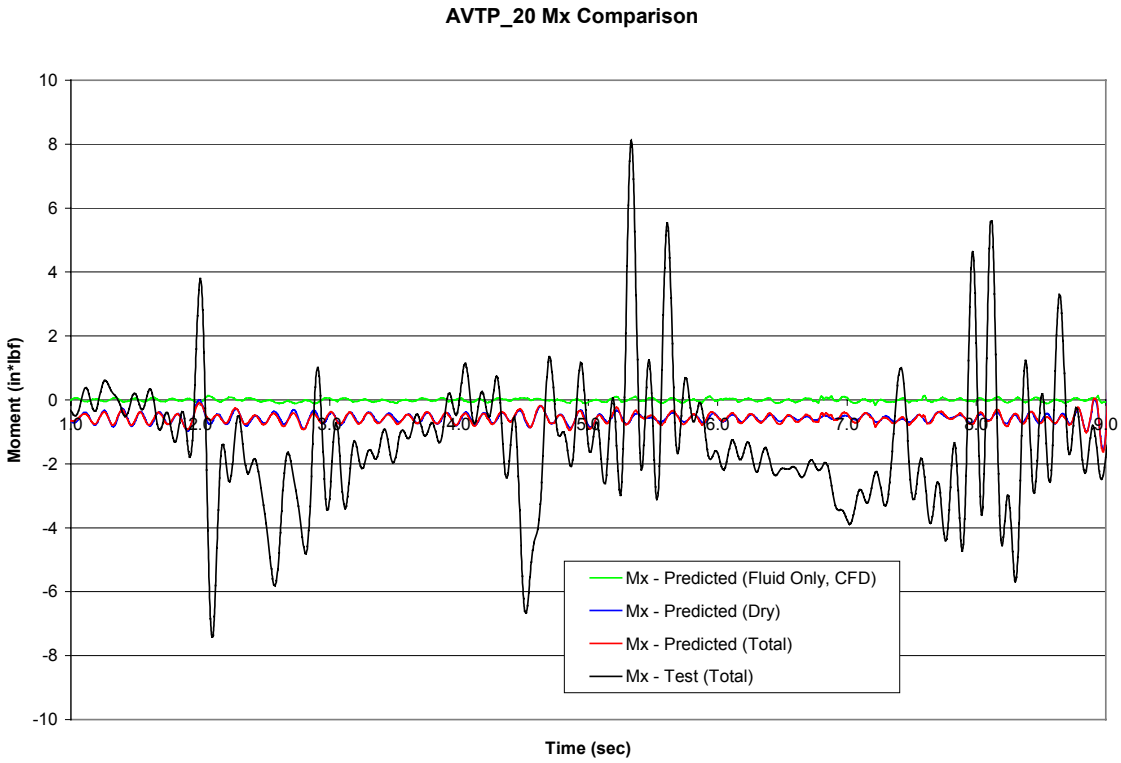
AVTP_20 Mx Comparison
Moment (in*lbf)
Time (sec)
Mx - Predicted (Fluid Only, CFD)
Mx - Predicted (Dry)
Mx - Predicted (Total)
Mx - Test (Total)

AVTP_20 My Comparison

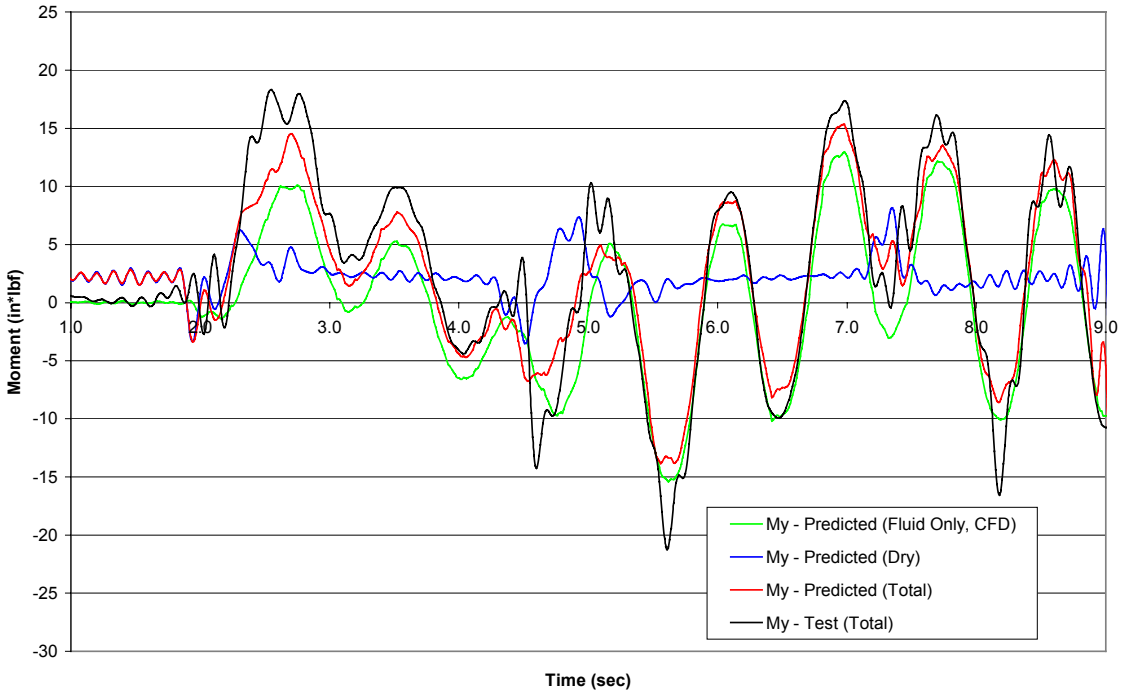

AVTP_20 Mz Comparison

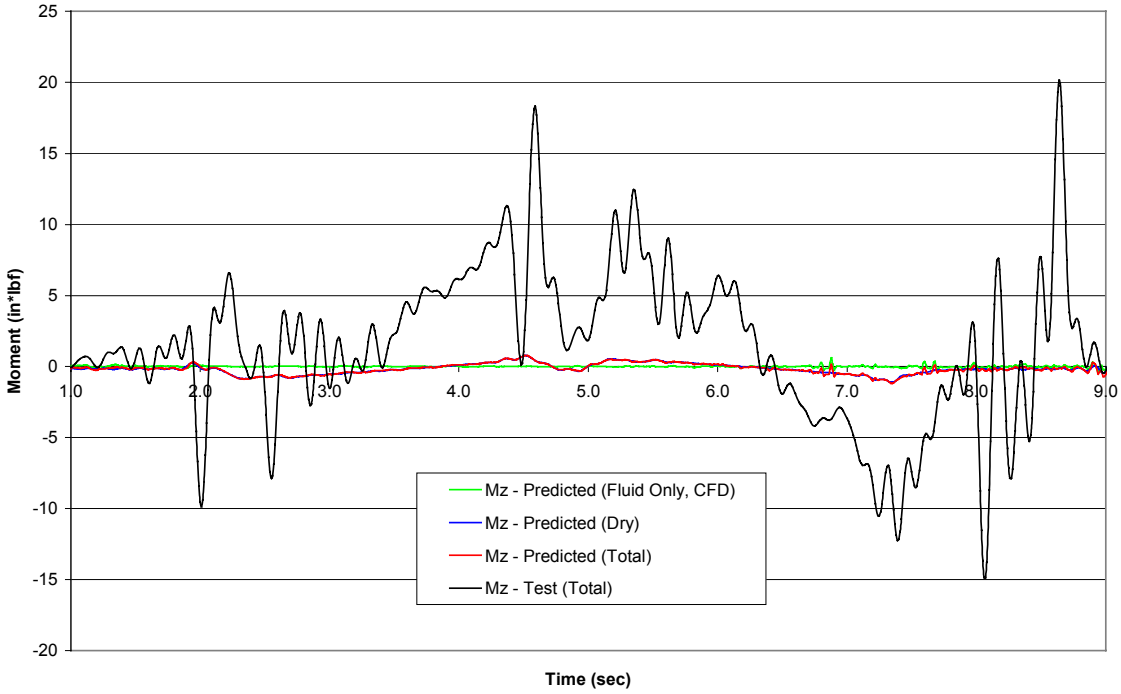

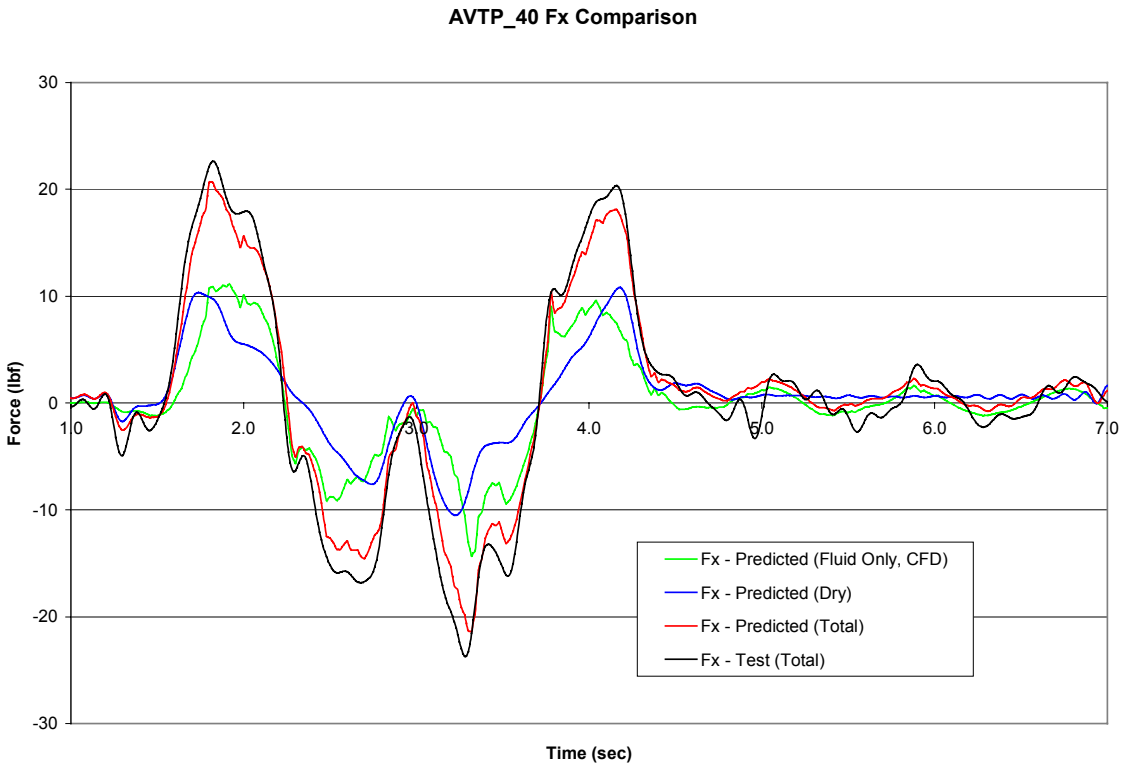
AVTP_40 Fx Comparison
Force (lbf)
Time (sec)
30
20
10
0
-10
-20
-30
1.0
2.0
3.0
4.0
5.0
6.0
7.0
Fx - Predicted (Fluid Only, CFD)
Fx - Predicted (Dry)
Fx - Predicted (Total)
Fx - Test (Total)

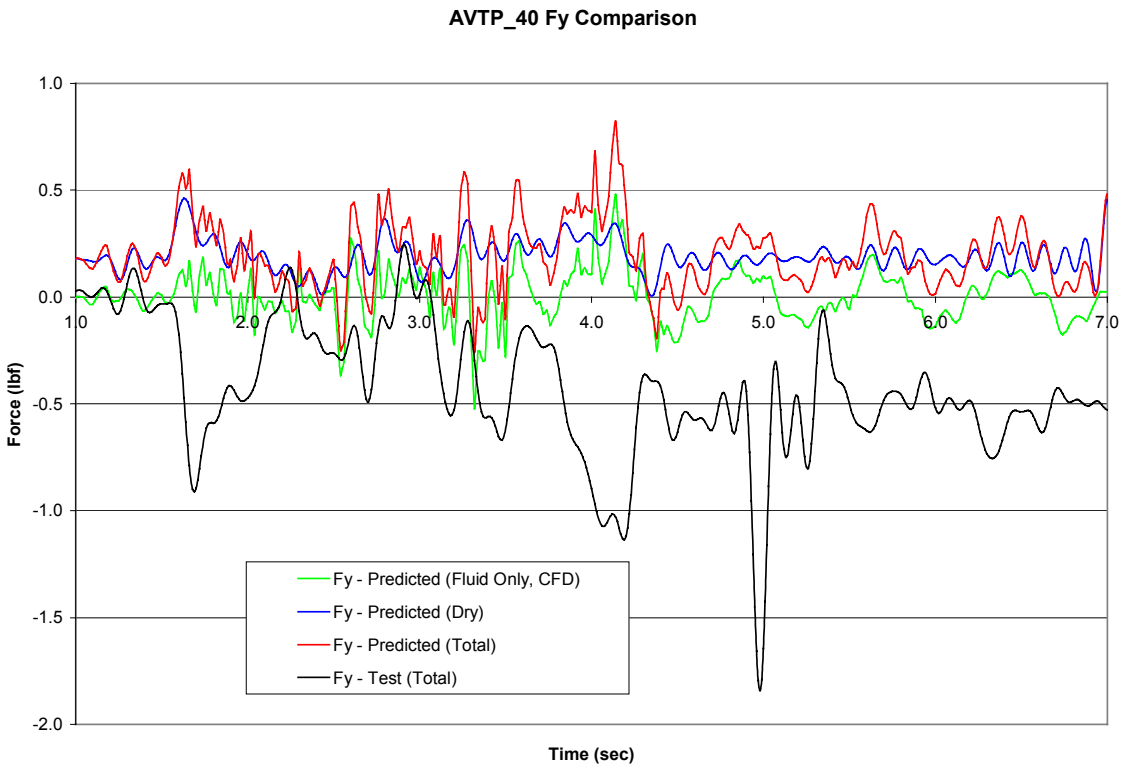
AVTP_40 Fy Comparison
Force (lbf)
Time (sec)
1.0
0.5
0.0
-0.5
-1.0
-1.5
-2.0
1.0
2.0
3.0
4.0
5.0
6.0
7.0
Fy - Predicted (Fluid Only, CFD)
Fy - Predicted (Dry)
Fy - Predicted (Total)
Fy - Test (Total)

AVTP_40 Fz Comparison

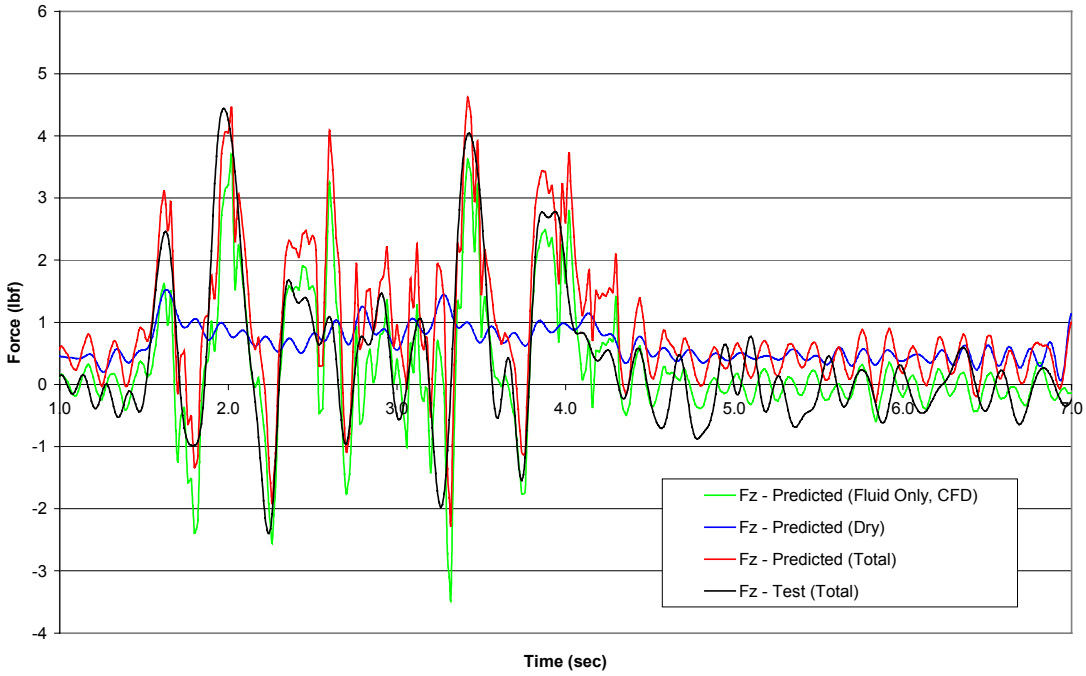

AVTP_40 Mx Comparison

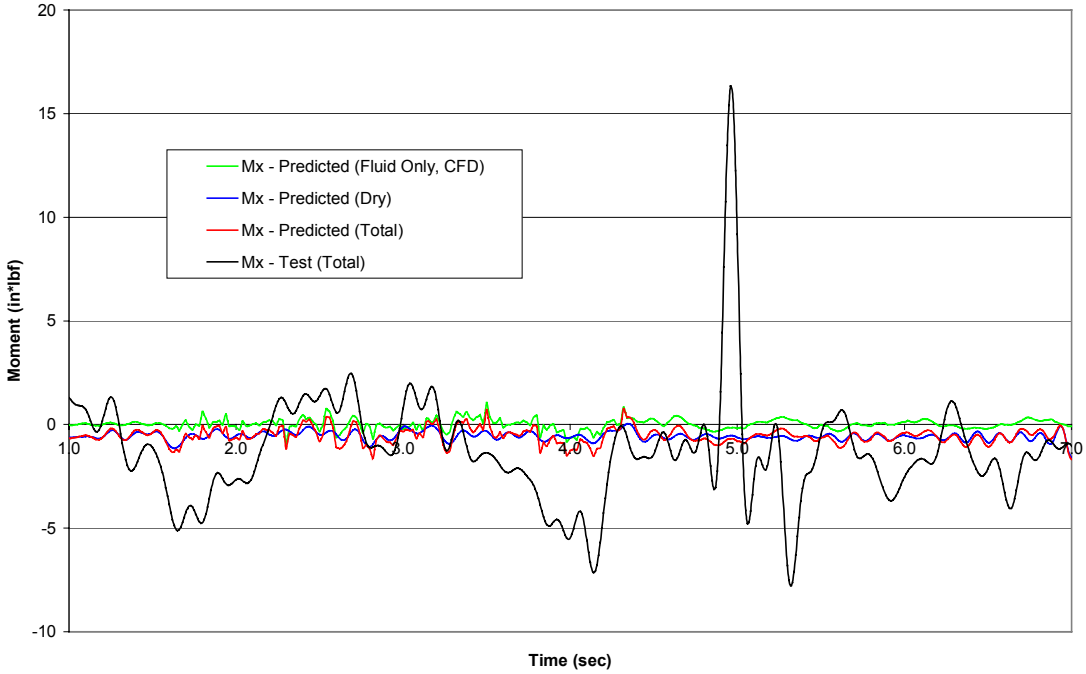

AVTP_40 My Comparison

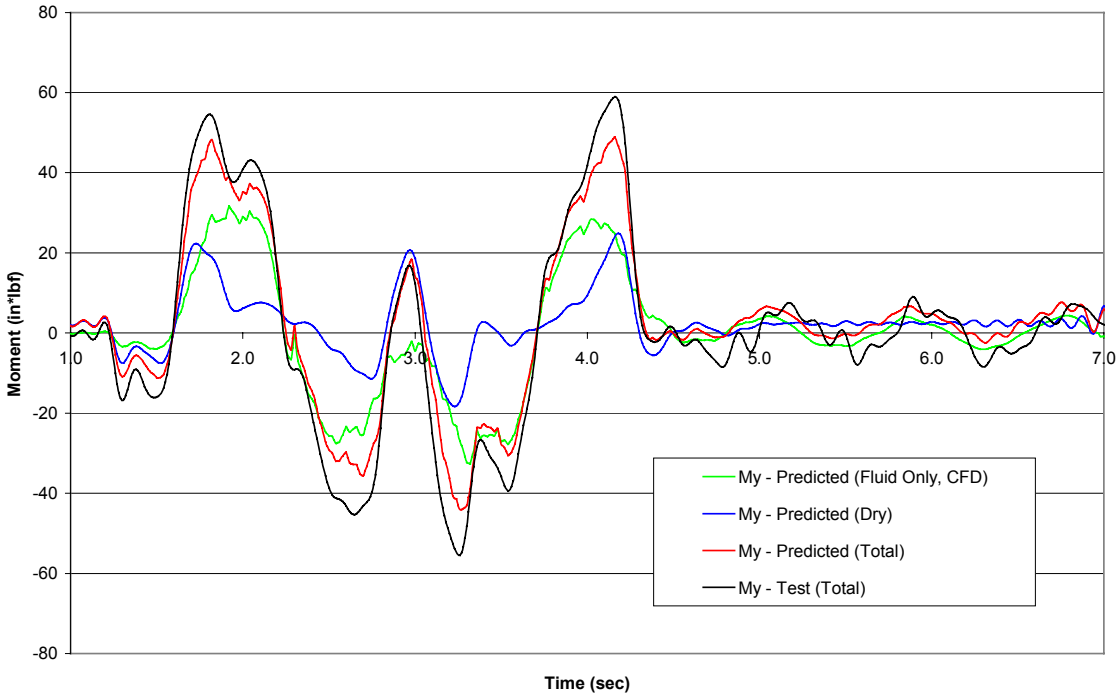

AVTP_40 Mz Comparison

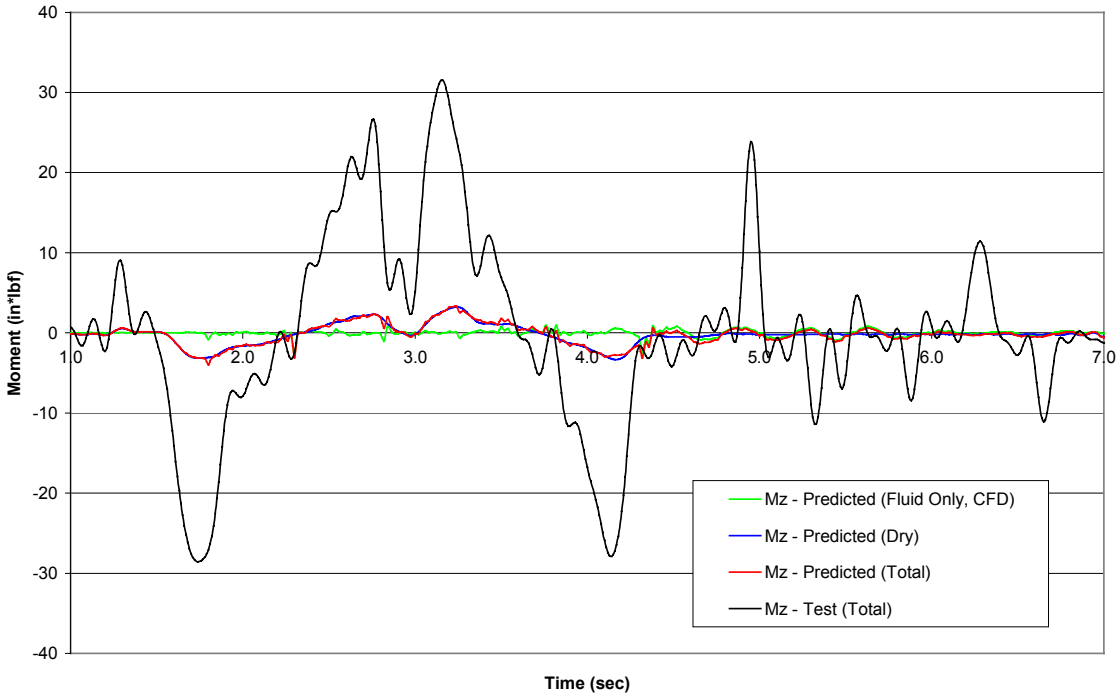

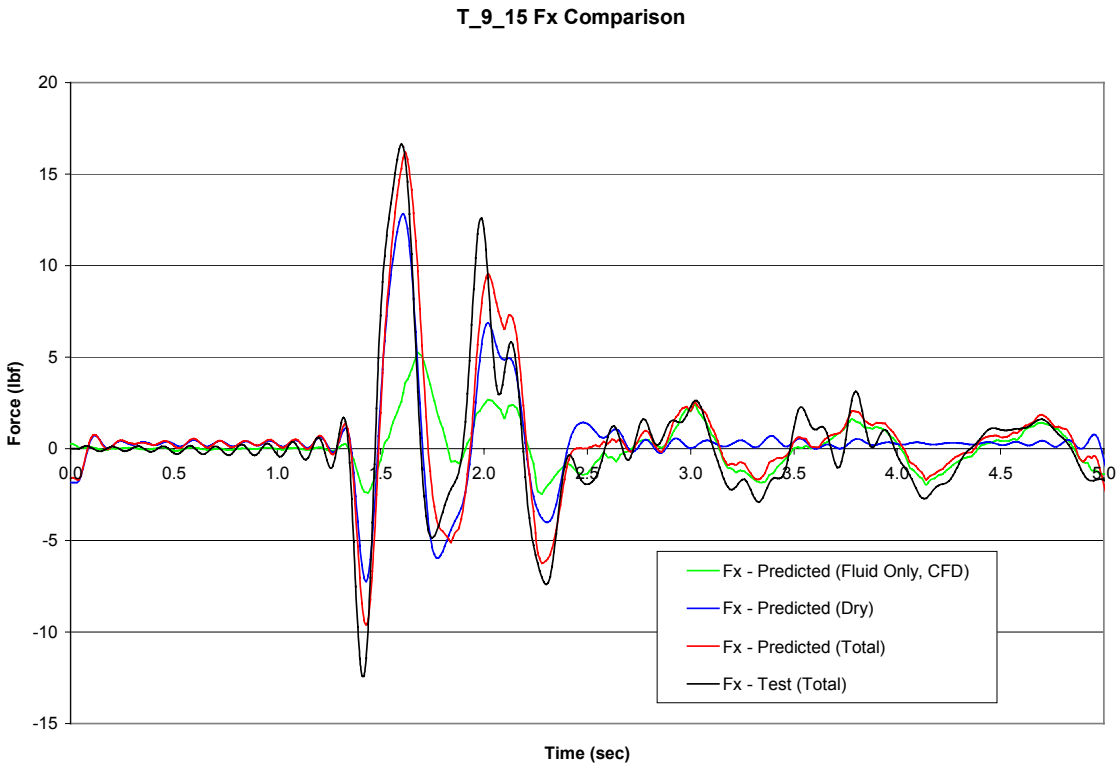
T_9_15 Fx Comparison
Force (lbf)
Time (sec)
Fx - Predicted (Fluid Only, CFD)
Fx - Predicted (Dry)
Fx - Predicted (Total)
Fx - Test (Total)

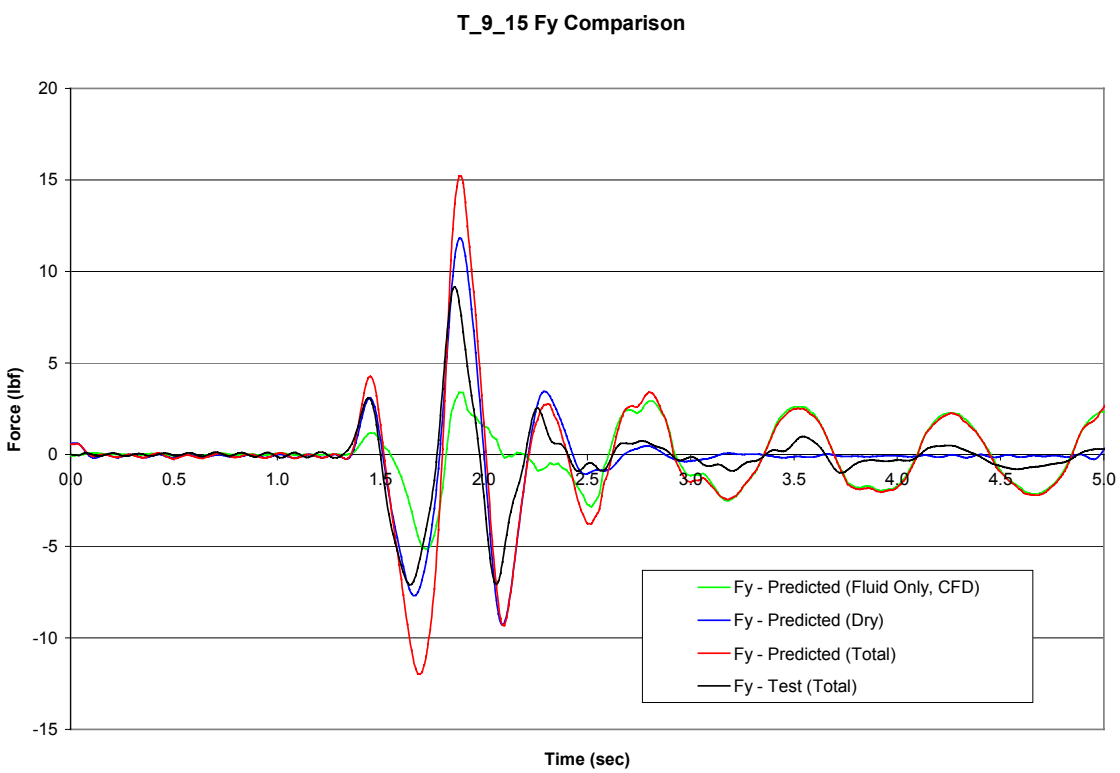
T_9_15 Fy Comparison
Force (lbf)
Time (sec)
Fy - Predicted (Fluid Only, CFD)
Fy - Predicted (Dry)
Fy - Predicted (Total)
Fy - Test (Total)

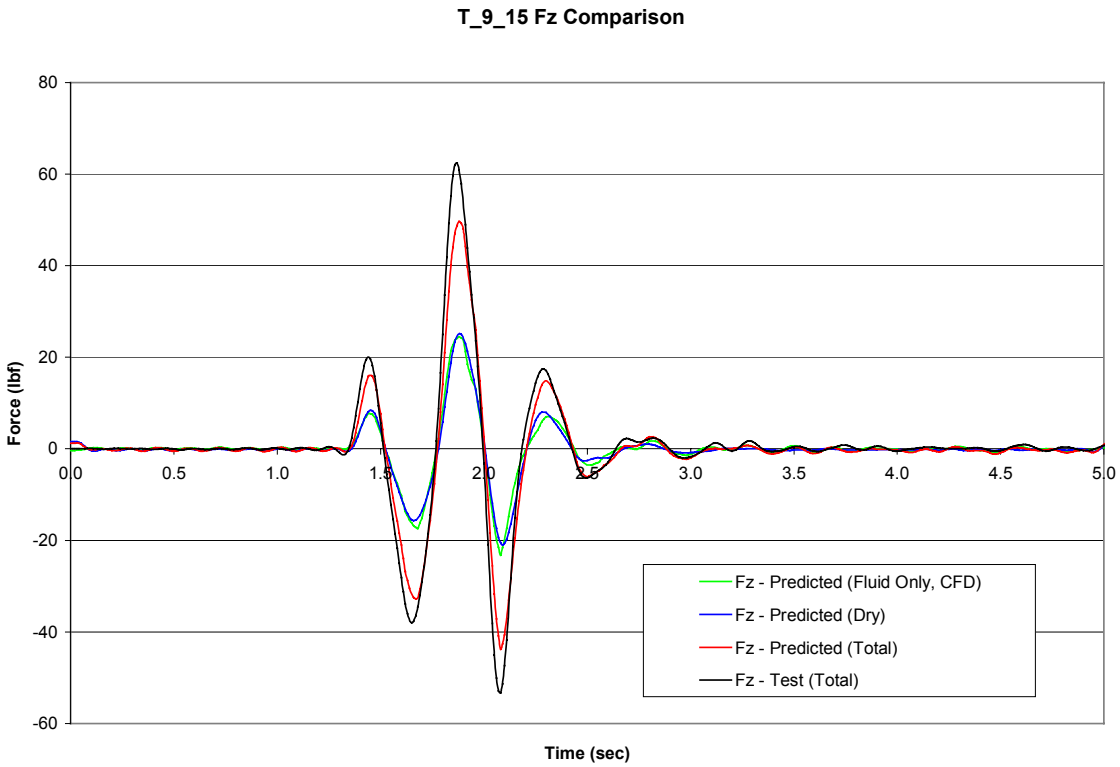
T_9_15 Fz Comparison
Force (lbf)
Time (sec)
80
60
40
20
0
-20
-40
-60
0.0
0.5
1.0
1.5
2.0
2.5
3.0
3.5
4.0
4.5
5.0
Fz - Predicted (Fluid Only, CFD)
Fz - Predicted (Dry)
Fz - Predicted (Total)
Fz - Test (Total)

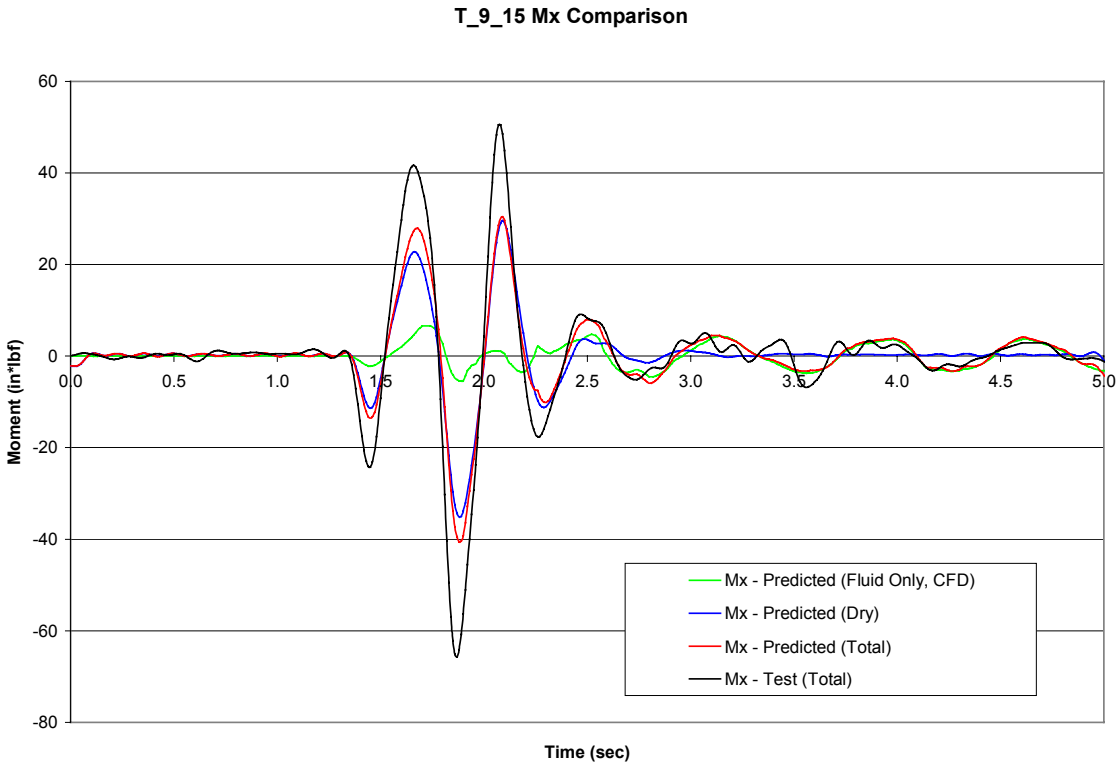
T_9_15 Mx Comparison
Moment (in*lbf)
Time (sec)
60
40
20
0
-20
-40
-60
-80
0.0
0.5
1.0
1.5
2.0
2.5
3.0
3.5
4.0
4.5
5.0
Mx - Predicted (Fluid Only, CFD)
Mx - Predicted (Dry)
Mx - Predicted (Total)
Mx - Test (Total)

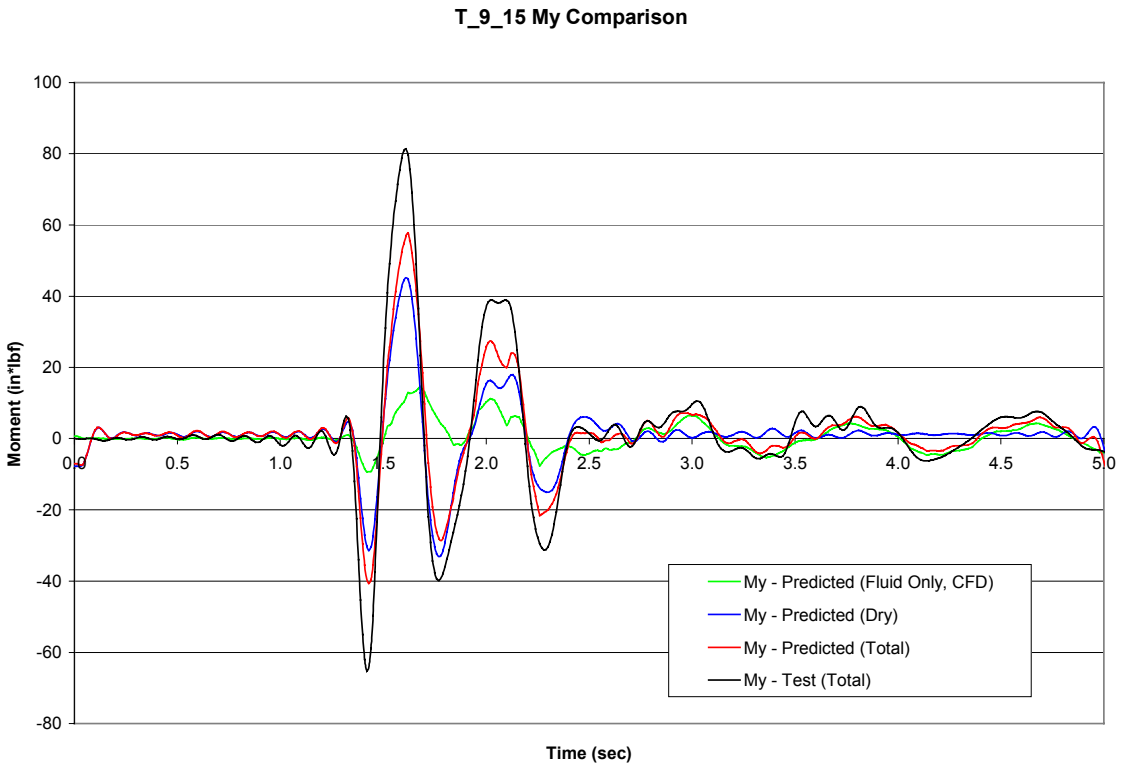
T_9_15 My Comparison
Moment (in*lbf)
Time (sec)
My - Predicted (Fluid Only, CFD)
My - Predicted (Dry)
My - Predicted (Total)
My - Test (Total)

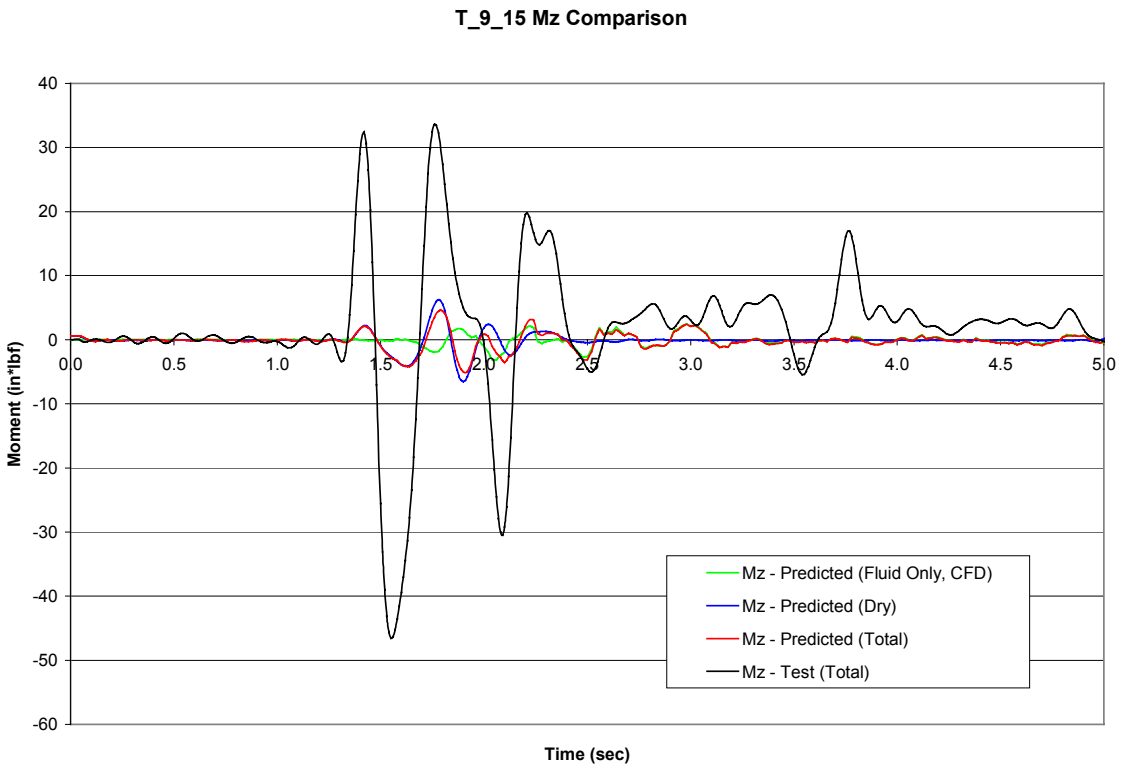
T_9_15 Mz Comparison
Moment (in*lbf)
Time (sec)
Mz - Predicted (Fluid Only, CFD)
Mz - Predicted (Dry)
Mz - Predicted (Total)
Mz - Test (Total)

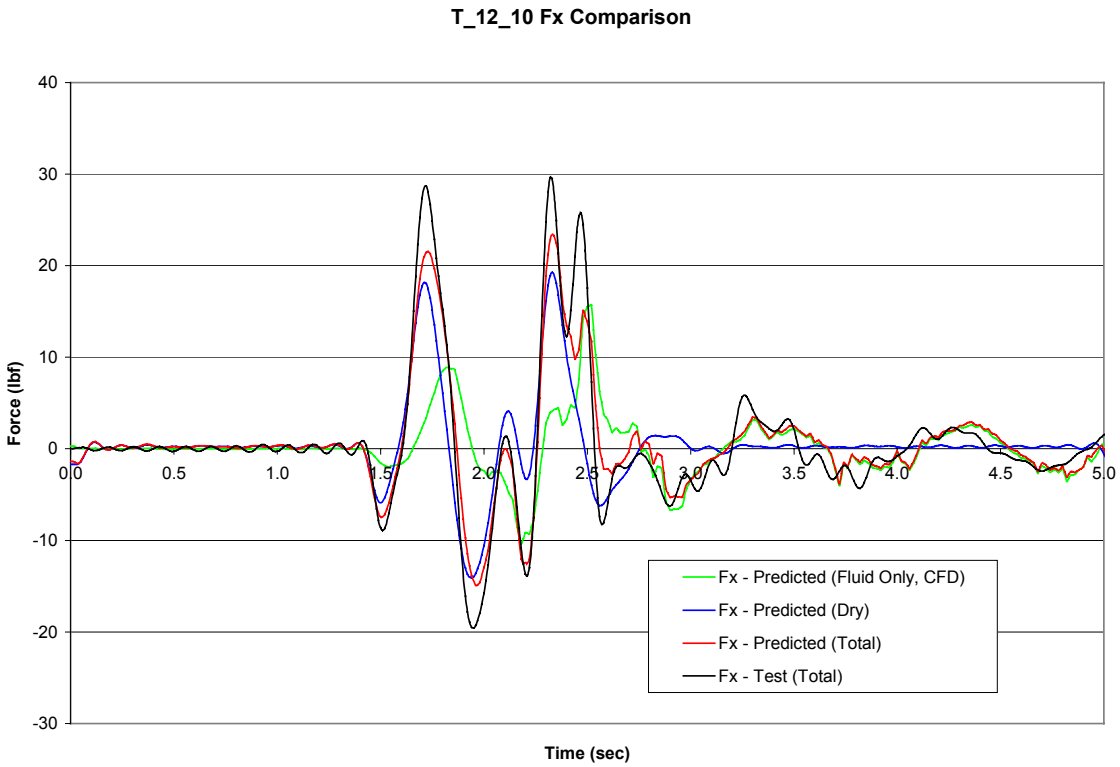
T_12_10 Fx Comparison
Force (lbf)
Time (sec)
Fx - Predicted (Fluid Only, CFD)
Fx - Predicted (Dry)
Fx - Predicted (Total)
Fx - Test (Total)

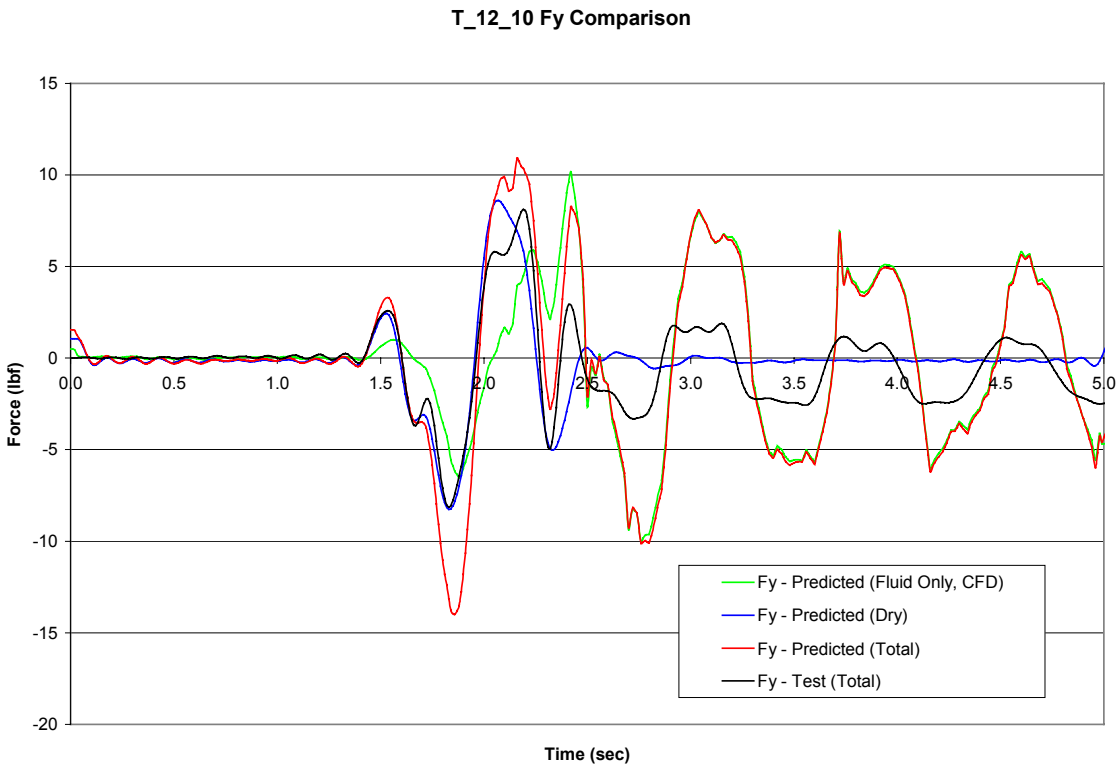
T_12_10 Fy Comparison
Force (lbf)
Time (sec)
Fy - Predicted (Fluid Only, CFD)
Fy - Predicted (Dry)
Fy - Predicted (Total)
Fy - Test (Total)

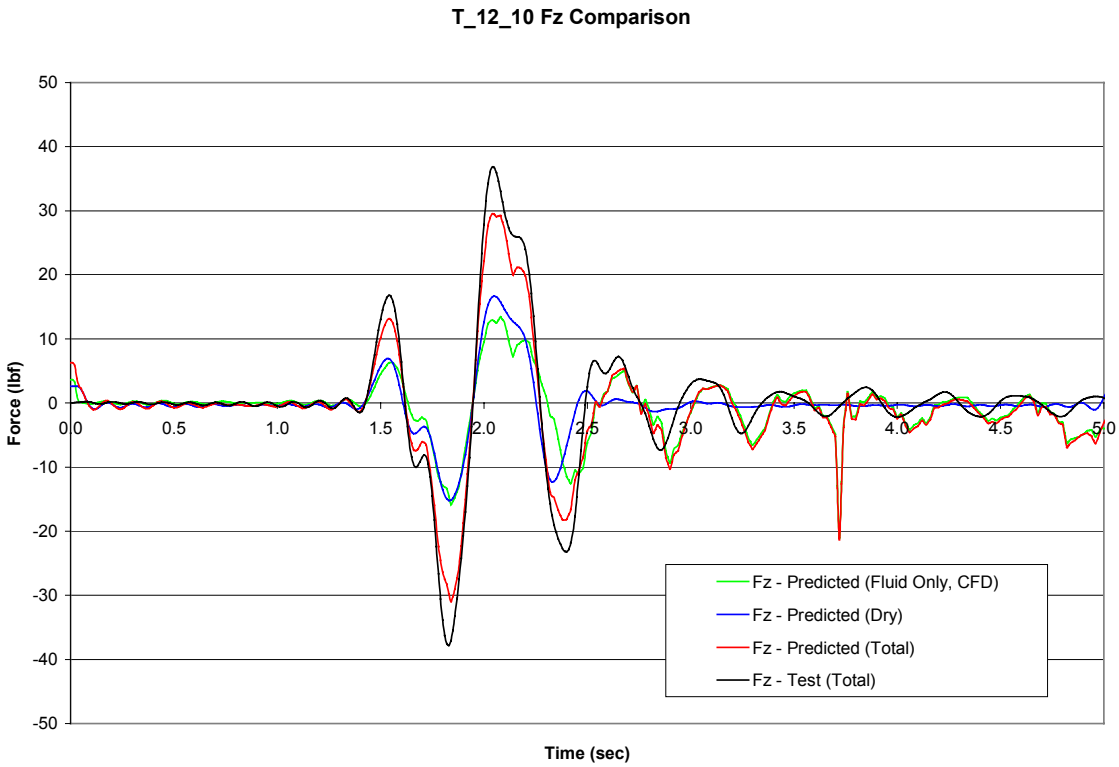
T_12_10 Fz Comparison
Force (lbf)
Time (sec)
Fz - Predicted (Fluid Only, CFD)
Fz - Predicted (Dry)
Fz - Predicted (Total)
Fz - Test (Total)

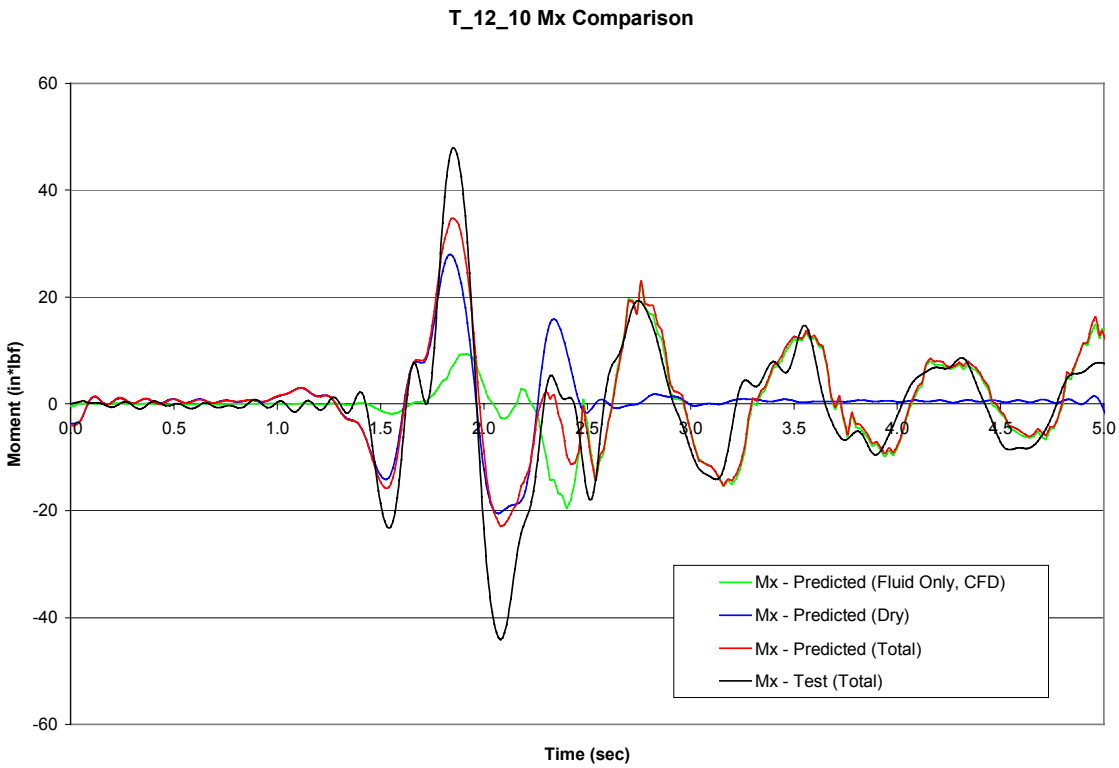
T_12_10 Mx Comparison
Moment (in*lbf)
Time (sec)
Mx - Predicted (Fluid Only, CFD)
Mx - Predicted (Dry)
Mx - Predicted (Total)
Mx - Test (Total)

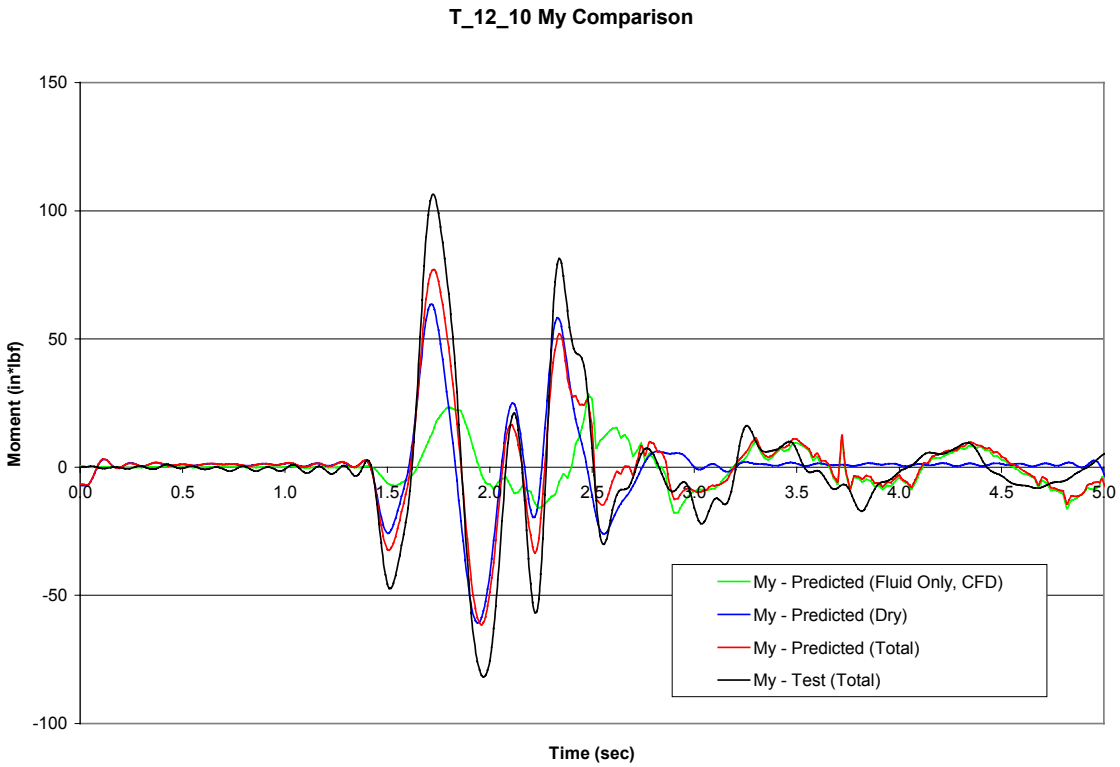
T_12_10 My Comparison
Moment (in*lbf)
Time (sec)
My - Predicted (Fluid Only, CFD)
My - Predicted (Dry)
My - Predicted (Total)
My - Test (Total)

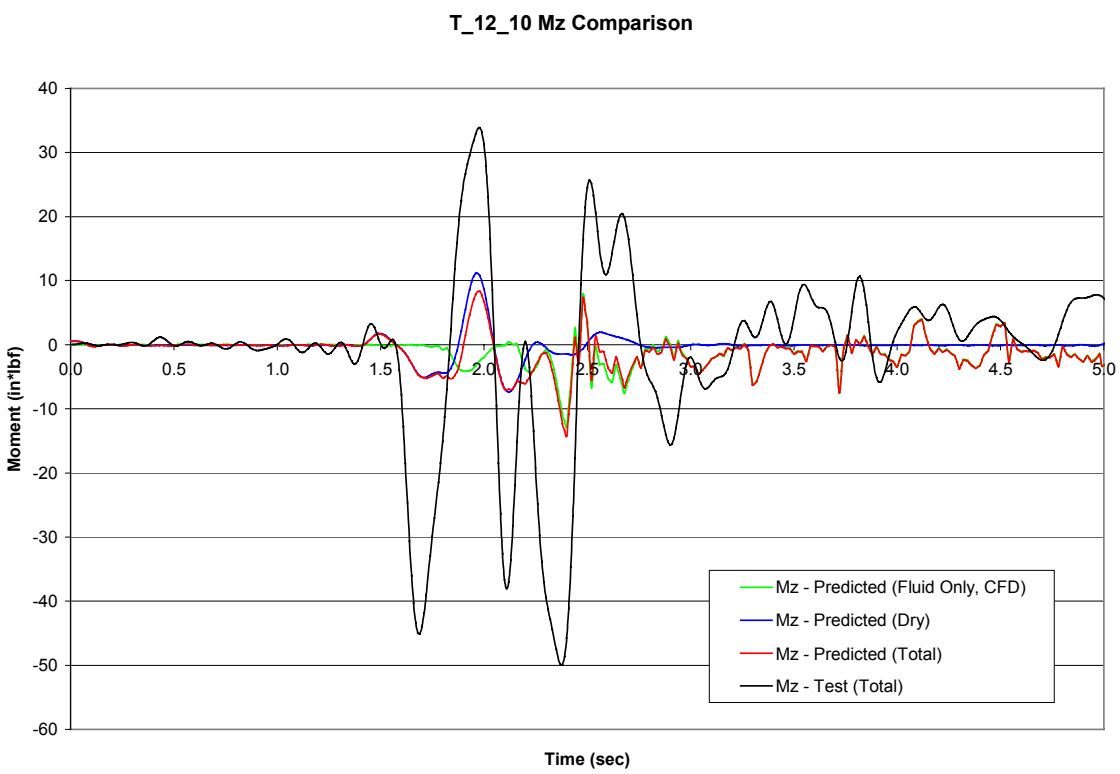
T_12_10 Mz Comparison
Moment (in*lbf)
Time (sec)
Mz - Predicted (Fluid Only, CFD)
Mz - Predicted (Dry)
Mz - Predicted (Total)
Mz - Test (Total)

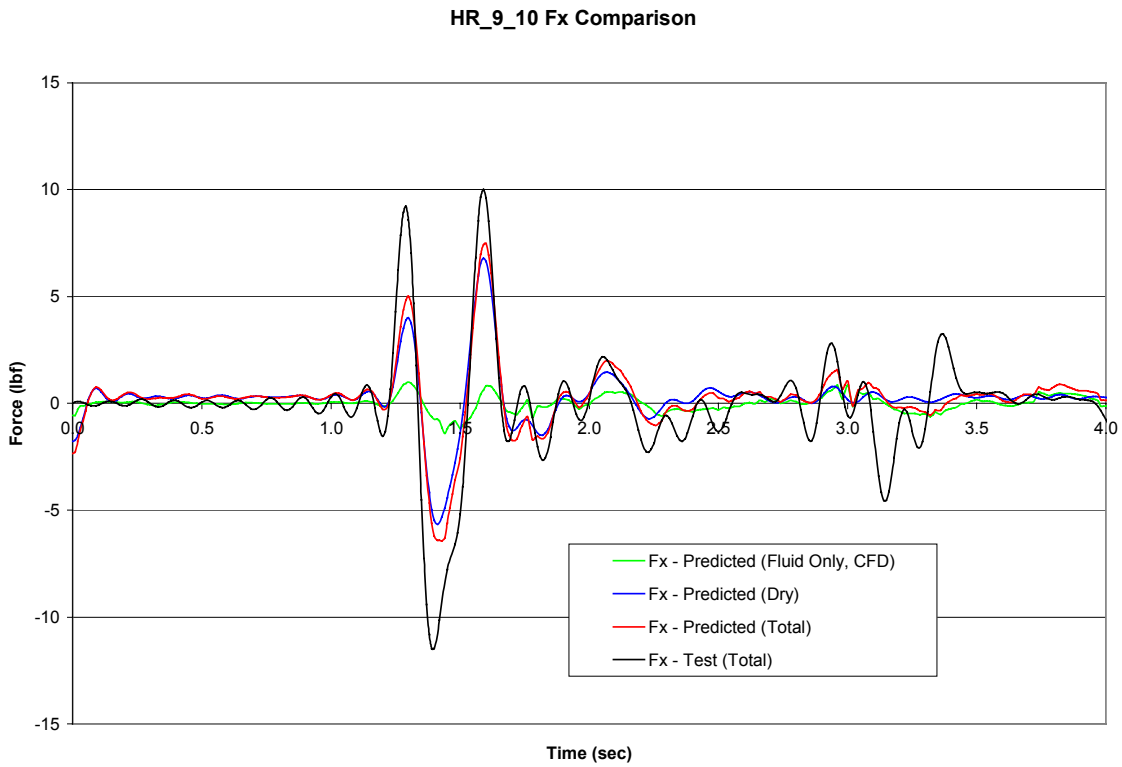
HR_9_10 Fx Comparison
Force (lbf)
Time (sec)
15
10
5
0
-5
-10
-15
0.0
0.5
1.0
1.5
2.0
2.5
3.0
3.5
4.0
Fx - Predicted (Fluid Only, CFD)
Fx - Predicted (Dry)
Fx - Predicted (Total)
Fx - Test (Total)

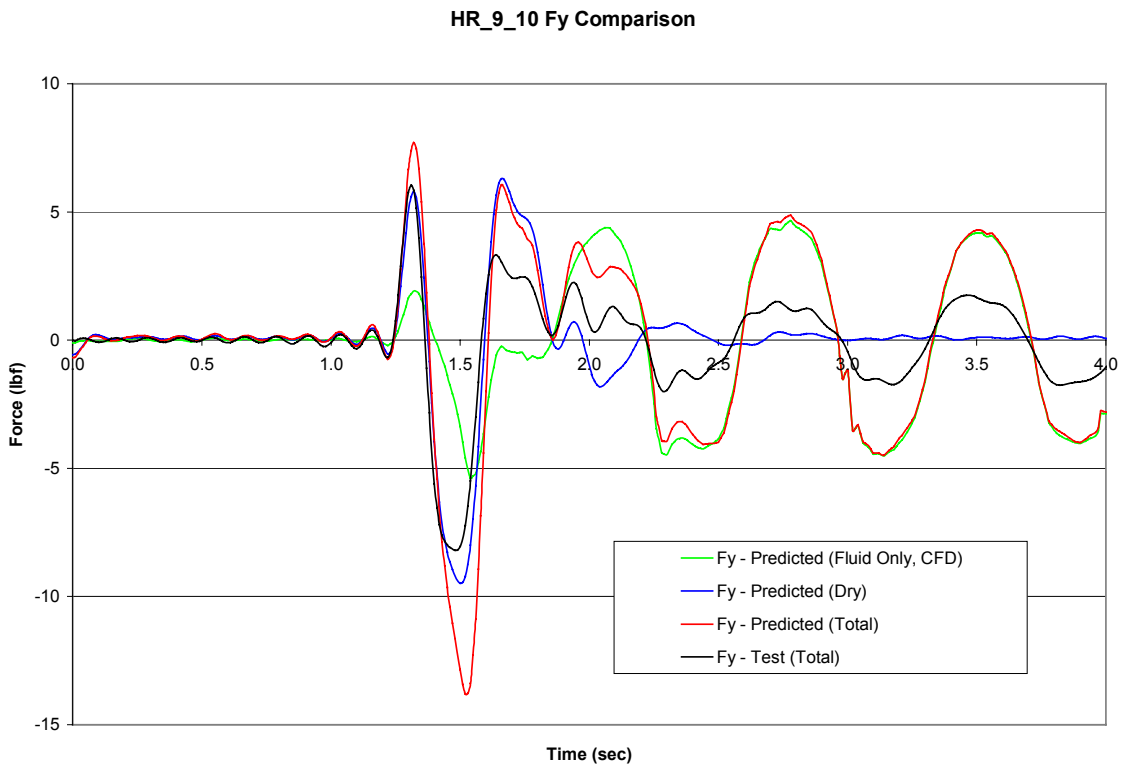
HR_9_10 Fy Comparison
Force (lbf)
Time (sec)
10
5
0
-5
-10
-15
0.0
0.5
1.0
1.5
2.0
2.5
3.0
3.5
4.0
Fy - Predicted (Fluid Only, CFD)
Fy - Predicted (Dry)
Fy - Predicted (Total)
Fy - Test (Total)

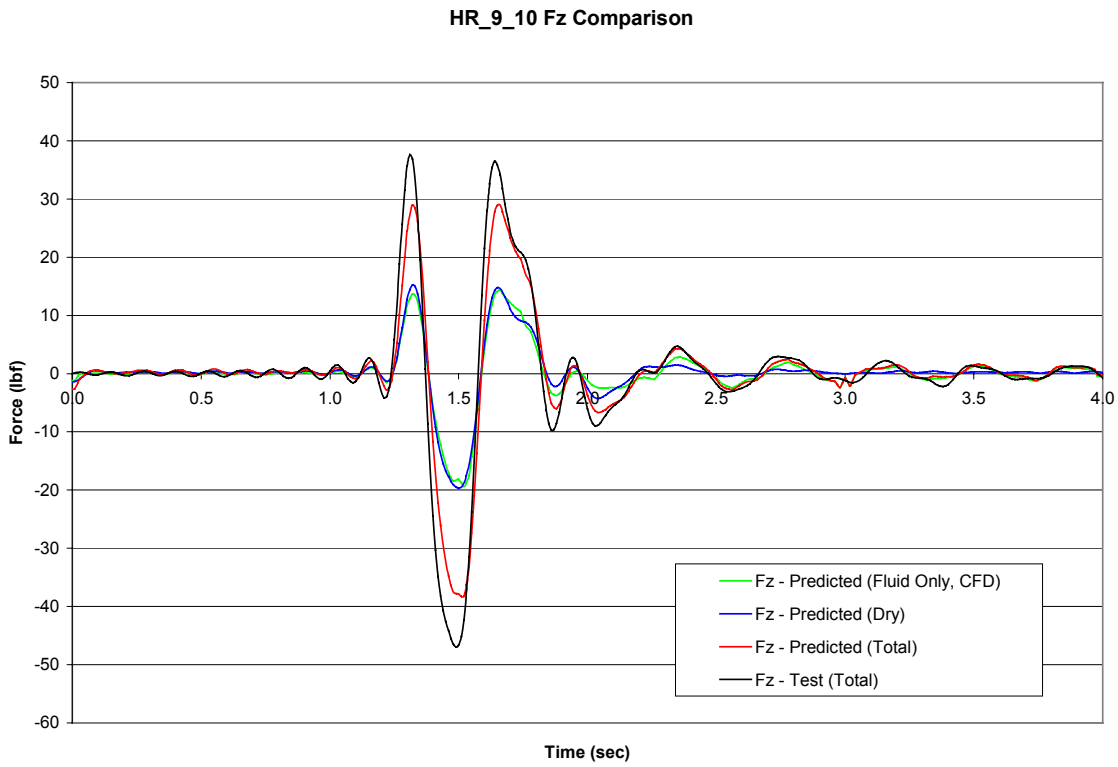
HR_9_10 Fz Comparison
Force (lbf)
Time (sec)
50
40
30
20
10
0
-10
-20
-30
-40
-50
-60
0.0
0.5
1.0
1.5
2.0
2.5
3.0
3.5
4.0
Fz - Predicted (Fluid Only, CFD)
Fz - Predicted (Dry)
Fz - Predicted (Total)
Fz - Test (Total)

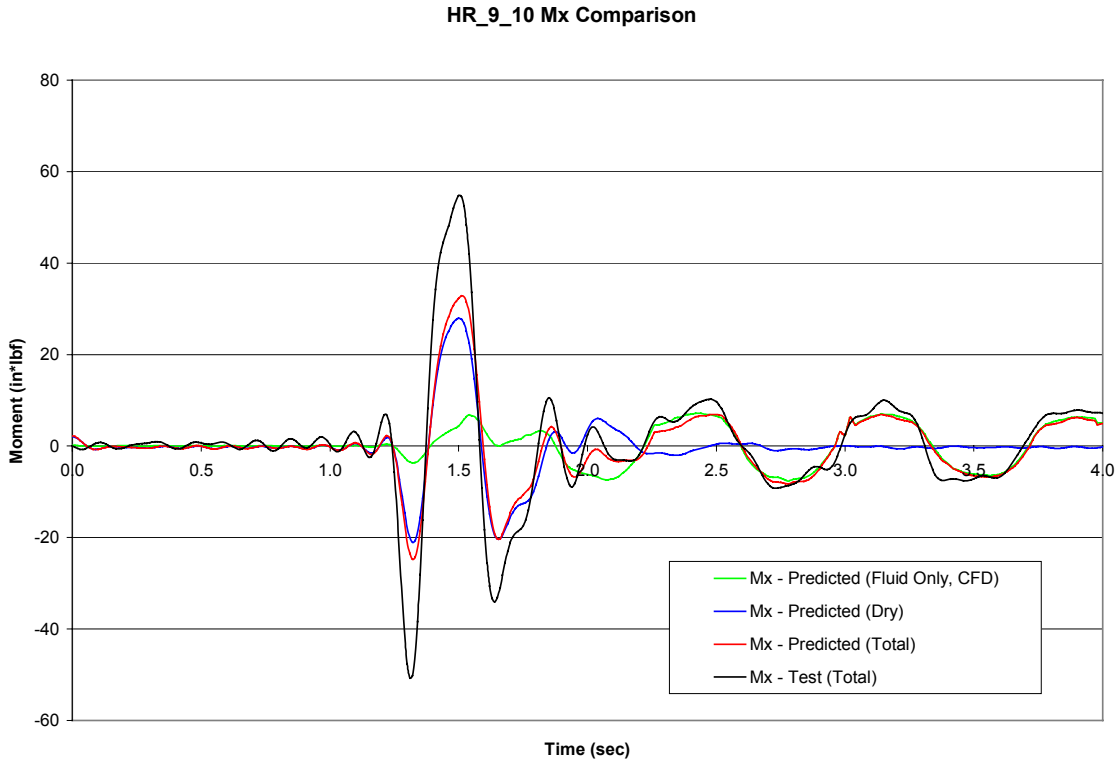
HR_9_10 Mx Comparison
Moment (in*lbf)
Time (sec)
80
60
40
20
0
-20
-40
-60
0.0
0.5
1.0
1.5
2.0
2.5
3.0
3.5
4.0
Mx - Predicted (Fluid Only, CFD)
Mx - Predicted (Dry)
Mx - Predicted (Total)
Mx - Test (Total)

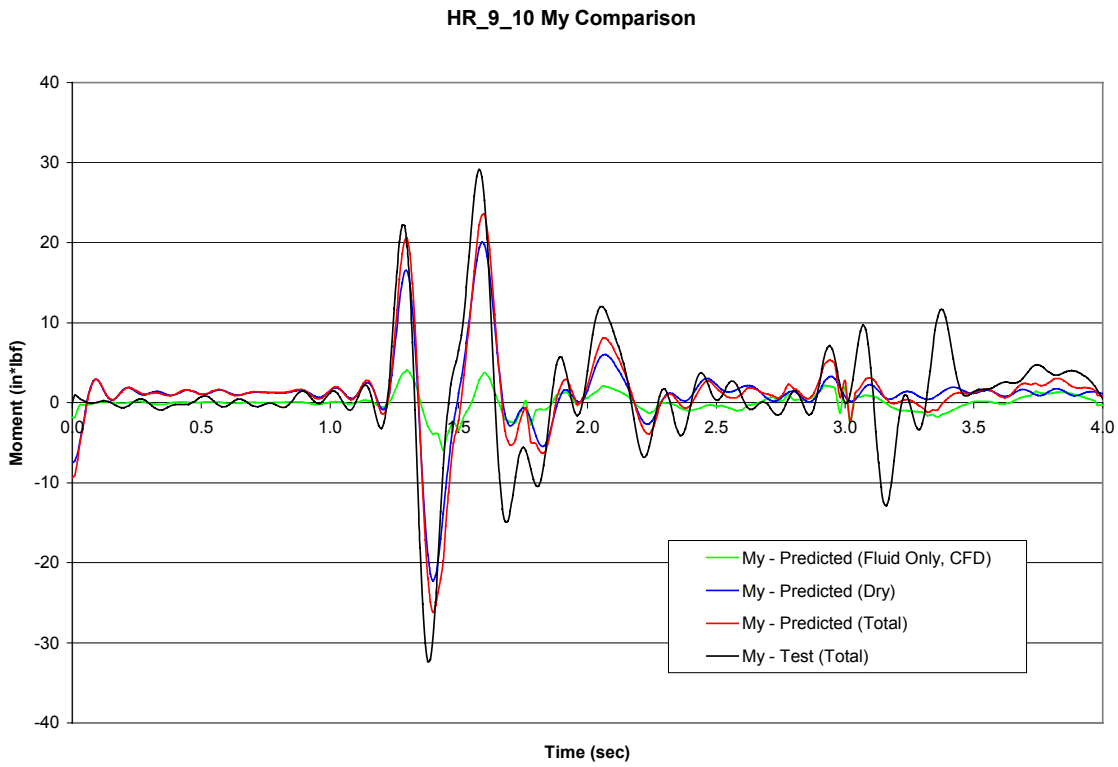
HR_9_10 My Comparison
Moment (in*lbf)
Time (sec)
My - Predicted (Fluid Only, CFD)
My - Predicted (Dry)
My - Predicted (Total)
My - Test (Total)

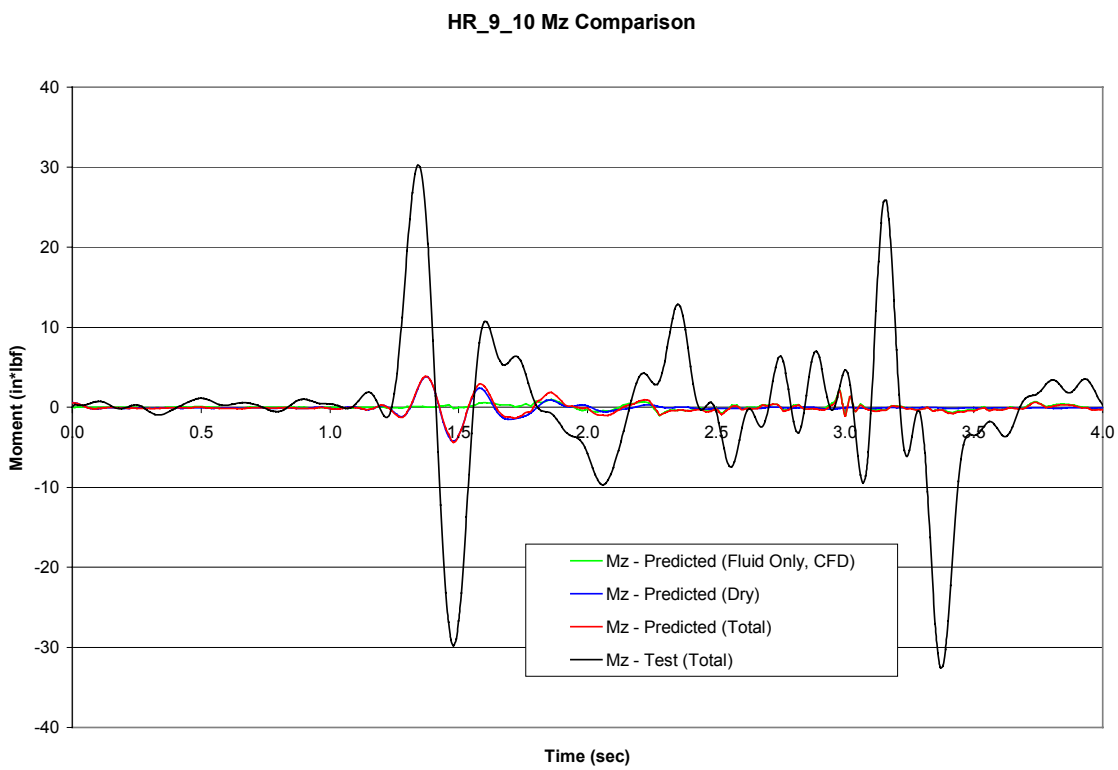
HR_9_10 Mz Comparison
Moment (in*lbf)
Time (sec)
Mz - Predicted (Fluid Only, CFD)
Mz - Predicted (Dry)
Mz - Predicted (Total)
Mz - Test (Total)

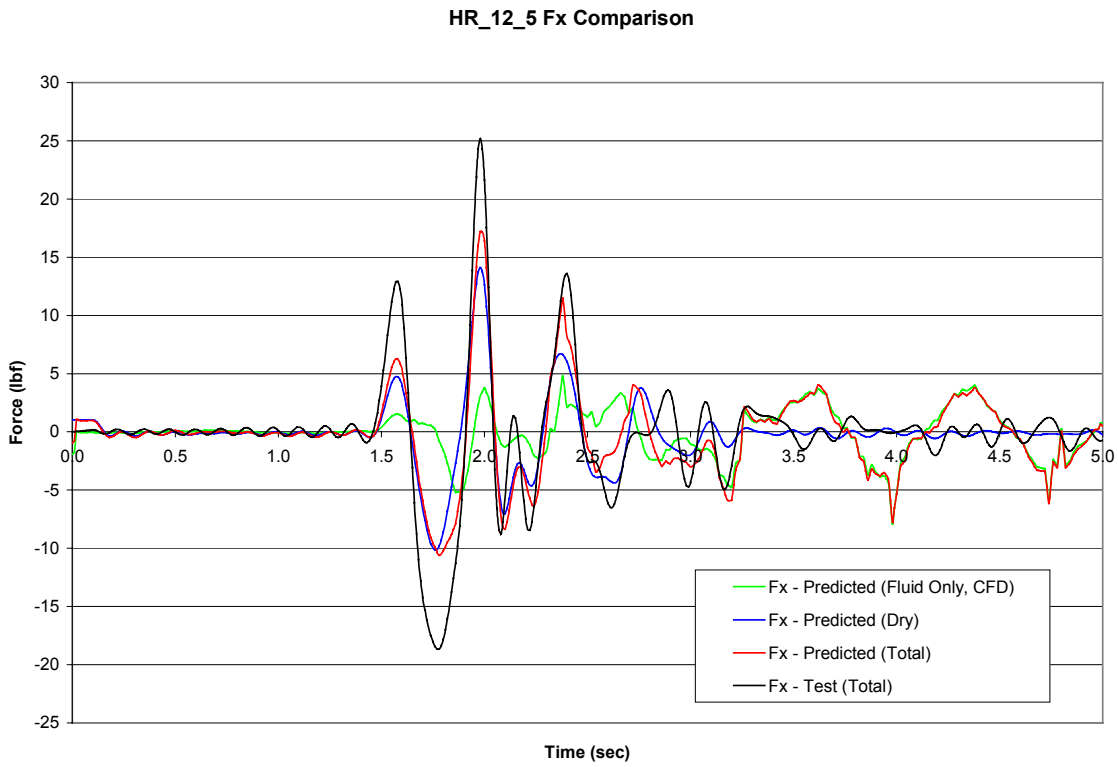
HR_12_5 Fx Comparison
Force (lbf)
Time (sec)
Fx - Predicted (Fluid Only, CFD)
Fx - Predicted (Dry)
Fx - Predicted (Total)
Fx - Test (Total)

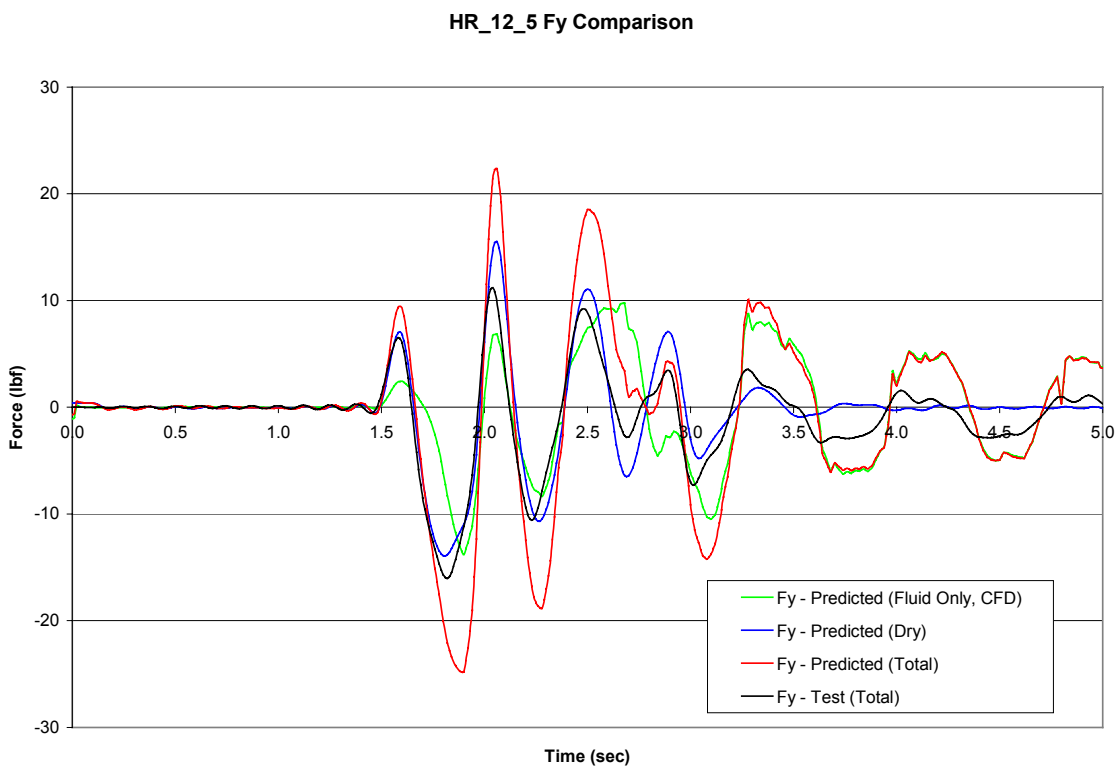
HR_12_5 Fy Comparison
Force (lbf)
Time (sec)
Fy - Predicted (Fluid Only, CFD)
Fy - Predicted (Dry)
Fy - Predicted (Total)
Fy - Test (Total)

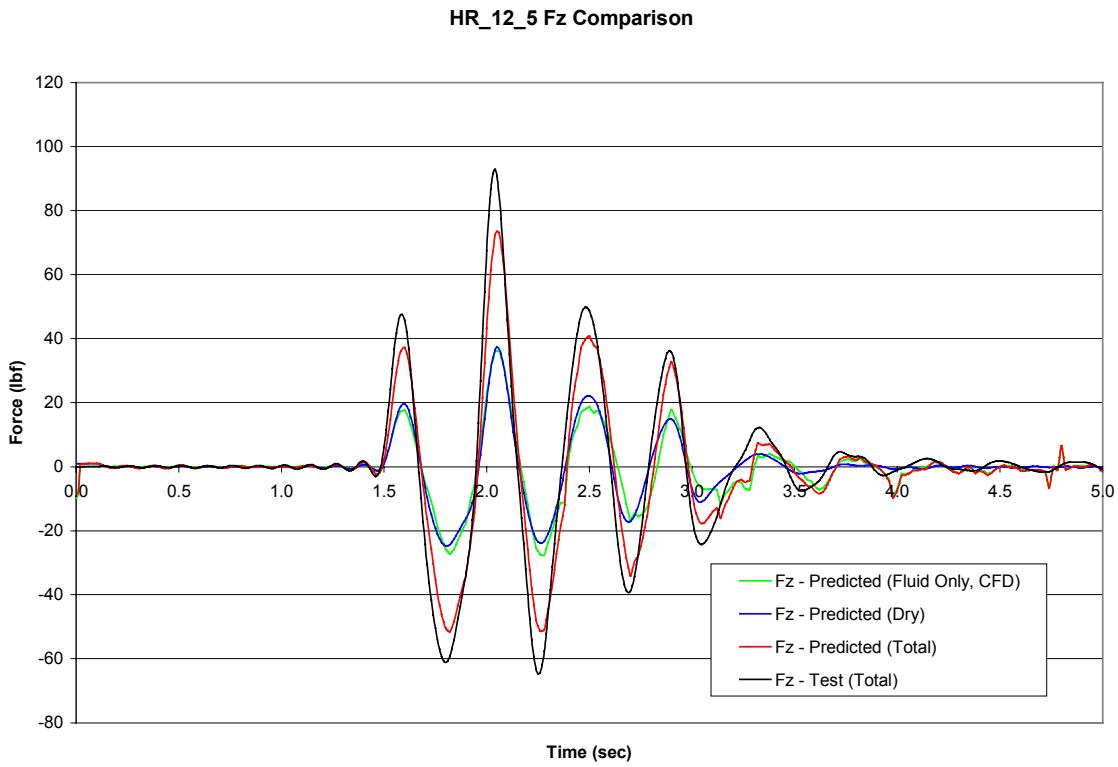
HR_12_5 Fz Comparison
Force (lbf)
Time (sec)
120
100
80
60
40
20
0
-20
-40
-60
-80
0.0
0.5
1.0
1.5
2.0
2.5
3.0
3.5
4.0
4.5
5.0
Fz - Predicted (Fluid Only, CFD)
Fz - Predicted (Dry)
Fz - Predicted (Total)
Fz - Test (Total)

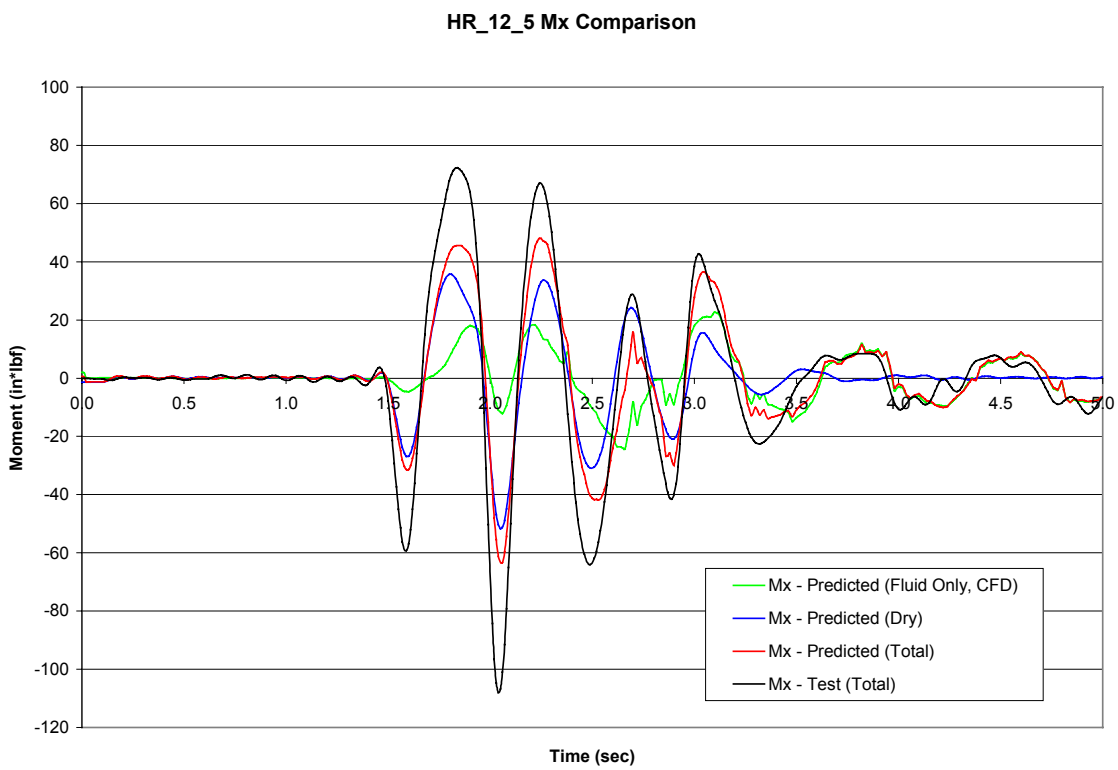
HR_12_5 Mx Comparison
Moment (in*lbf)
Time (sec)
100
80
60
40
20
0
-20
-40
-60
-80
-100
-120
0.0
0.5
1.0
1.5
2.0
2.5
3.0
3.5
4.0
4.5
5.0
Mx - Predicted (Fluid Only, CFD)
Mx - Predicted (Dry)
Mx - Predicted (Total)
Mx - Test (Total)

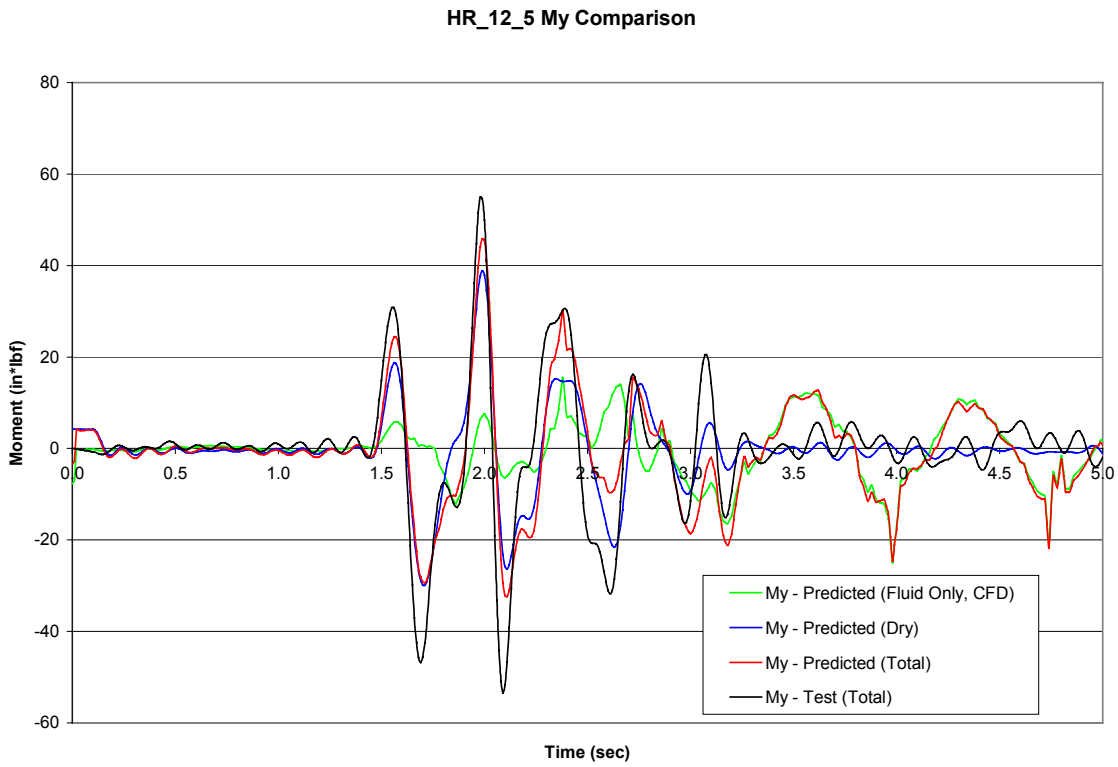
HR_12_5 My Comparison
Moment (in*lbf)
Time (sec)
My - Predicted (Fluid Only, CFD)
My - Predicted (Dry)
My - Predicted (Total)
My - Test (Total)

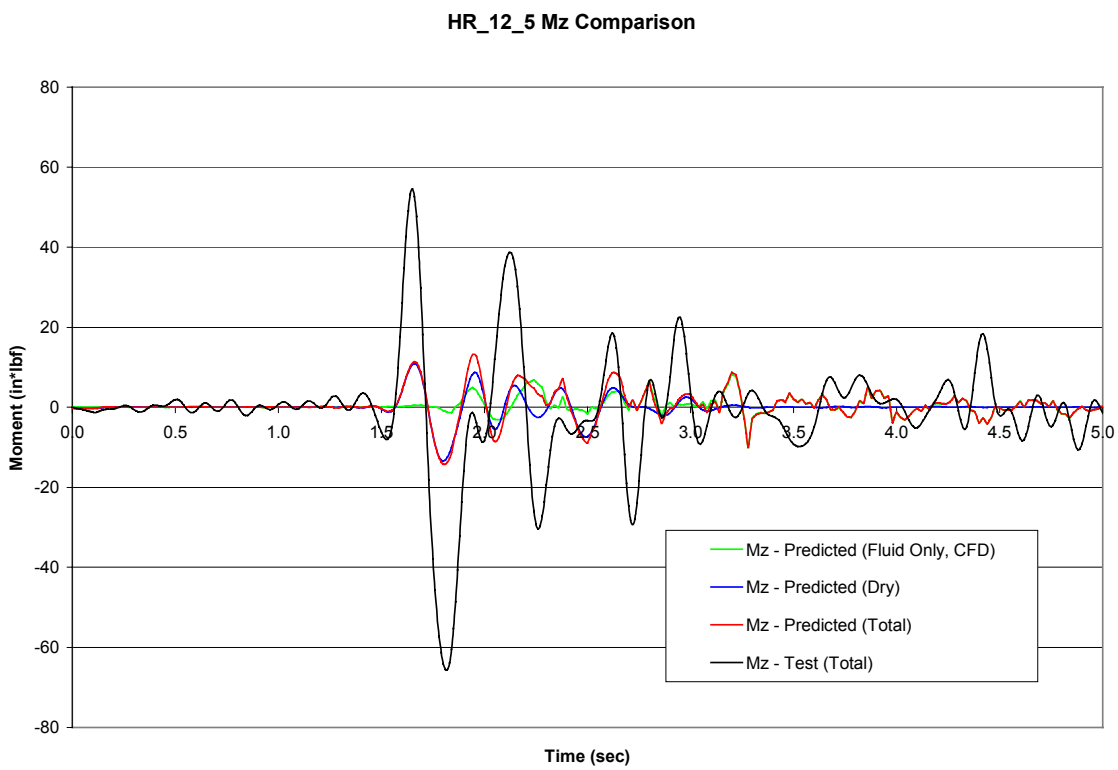
HR_12_5 Mz Comparison
Moment (in*lbf)
Time (sec)
Mz - Predicted (Fluid Only, CFD)
Mz - Predicted (Dry)
Mz - Predicted (Total)
Mz - Test (Total)